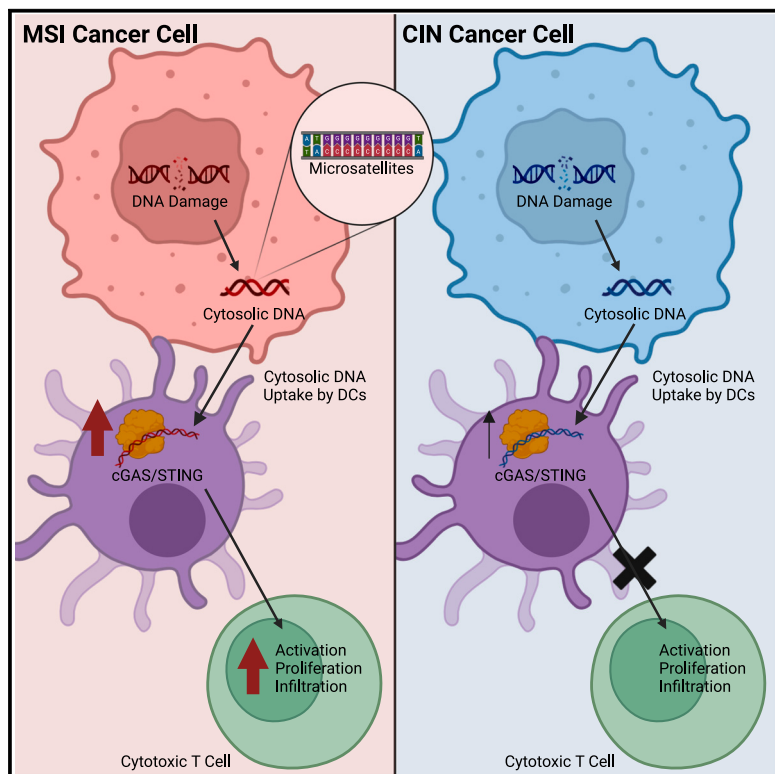


Cytosolic DNA composition is determined by genomic instability mechanism and regulates dendritic cell-mediated anti-tumor immunity

Graphical abstract



Authors

Shayla R. Mosley, Angie Chen,
David N.W. Doell, ...,
Felix Meier-Stephenson,
Vanessa Meier-Stephenson, Kristi Baker

Correspondence

mosley@ualberta.ca (S.R.M.),
kbaker2@alberta.ca (K.B.)

In brief

Mosley et al. find that strongly immunogenic cancers with MSI produce cytosolic DNA (cyDNA) more effective at promoting STING-mediated anti-tumor immune responses than those with CIN. Highly stimulatory cyDNAs produced by MSI and DNA-damaging therapies contain specific features, including microsatellites, increased size, and mitochondrial cyDNA, that strongly activate STING and enhance anti-tumor immunity.

Highlights

- Colorectal cancers with MSI induce cytosolic DNA enriched in potent STING-activating features
- DNA-damaging therapies like radiation and oxaliplatin produce highly stimulatory cytosolic DNA
- Radiation increases cytosolic DNA size and mitochondrial DNA release to boost STING activation
- Microsatellites in MSI CRC cytosolic DNA improve T cell responses in poorly immunogenic tumors



Article

Cytosolic DNA composition is determined by genomic instability mechanism and regulates dendritic cell-mediated anti-tumor immunity

Shayla R. Mosley,^{1,*} Angie Chen,¹ David N.W. Doell,¹ Siwon Choi,¹ Courtney Mowat,¹ Felix Meier-Stephenson,² Vanessa Meier-Stephenson,² and Kristi Baker^{1,2,3,*}

¹Department of Oncology, Cross Cancer Institute, University of Alberta, Edmonton, AB T6G 1Z2, Canada

²Department of Medical Microbiology and Immunology, University of Alberta, Edmonton, AB T6G 2R3, Canada

³Lead contact

*Correspondence: mosley@ualberta.ca (S.R.M.), kbaker2@alberta.ca (K.B.)

<https://doi.org/10.1016/j.celrep.2024.115177>

SUMMARY

Patients with colorectal cancers (CRCs) that have microsatellite instability (MSI) (MSI CRCs) face a better prognosis than those with the more common chromosomal instability (CIN) subtype (CIN CRCs) due to improved T cell-mediated anti-tumor immune responses. Previous investigations identified the cytosolic DNA (cyDNA) sensor STING as necessary for chemokine-mediated T cell recruitment in MSI CRCs. Here, we find that cyDNA from MSI CRC cells is inherently more capable of inducing STING activation and improves cytotoxic T cell activation by dendritic cells (DCs). Sequencing indicates that MSI cyDNA is enriched in microsatellites, which, upon DC uptake, induce anti-tumor immunity in a manner consistent with clinical MSI CRCs. DNA-damaging therapies also modulate cyDNA stimulation capacity, with radiation inducing larger cyDNA sizes and increased mitochondrial DNA content. Identifying highly stimulatory endogenous cyDNAs such as those in MSI CRCs will allow for optimized development of DNA-based STING agonist therapies to improve the responses of CIN CRCs with CIN to immunotherapies.

INTRODUCTION

Colorectal cancer (CRC) is the second most deadly cancer worldwide, with an estimated 1.9 million people diagnosed per year.¹ The majority of CRCs are initiated by mutations in *APC* and subsequently acquire mutations in *KRAS*, *BRAF*, *PTEN*, *RAD51*, and *TP53*, leading to chromosomal instability (CIN).^{2–4} Alternatively, 12%–15% of CRCs are established by transcriptional silencing of *MLH1*, leading to dysfunctional mismatch repair and high levels of point mutations and frameshifts in microsatellite regions of the genome, resulting in microsatellite instability (MSI).⁵ Clinically, patients with MSI CRCs face a better prognosis, with an estimated 35% lower risk of death.⁶ This can be attributed to their potent anti-tumor immunity characterized by high CD8⁺ cytotoxic T cell infiltration.⁷ While this has been linked to high neoantigen production due to the hypermutability of MSI CRCs,⁵ this theory is incomplete and fails to explain how microsatellite-unstable tumors in other organs are associated with a worse prognosis than comparable tumors without MSI.⁸ This indicates that neoantigen-independent mechanisms are an important feature of anti-tumor immunity in MSI CRCs. Previously, our lab identified high production of the T cell-recruiting chemokines CCL5 and CXCL10 as essential for the increased T cell activation and infiltration of MSI CRCs and showed that their expression is dependent on activation of the cytosolic DNA (cyDNA) sensor STING.⁹

STING is a pattern recognition receptor (PRR) that evolved to recognize microbial DNA in the cytosol.¹⁰ Sensing of cyDNA by cGAS induces its oligomerization and production of the cyclic dinucleotide 2'3'-cGAMP.^{11,12} 2'3'-cGAMP then activates STING, which forms a complex with TBK1 and IRF3, each of which are then phosphorylated by TBK1.¹³ pIRF3 then translocates to the nucleus to transcribe the type I interferons (IFNs) IFN α and IFN β , which then induce expression of IFN-stimulated genes, such as CCL5, CXCL10, and IRF7, through the JAK/STAT pathway.^{10,14} cGAS can also be activated by endogenous DNA that leaks into the cytosol following DNA damage.¹⁴ This has broad implications for cancers with genomic instability or those treated with DNA-damaging therapies. Indeed, STING has been shown to play a role in cancer prevention¹⁵ and the response to DNA-damaging treatments like ionizing radiation (IR).¹⁶ As such, STING agonists are currently in clinical trials alone or in combination with checkpoint inhibitors like pembrolizumab.¹⁷

Dendritic cells (DCs) are key mediators of both anti-tumor immunity and STING-dependent immune responses.¹² Exogenous type I IFN leads to DC activation, allowing for co-stimulation and cross-presentation to CD8⁺ T cells.¹² Recently, DCs have been shown to uptake cyDNA and 2'3'-cGAMP from tumor cells by phagocytosis, the formation of gap junctions, and uptake of cyDNA-containing exosomes, leading to STING activation and type I IFN production from within the DCs themselves.^{18,19}



Although we previously identified STING activation as a neo-antigen-independent mechanism of T cell infiltration and activation in MSI CRCs, we observed no significant difference in cy-DNA quantity between cells with MSI and CIN and proposed that there could instead be differences in the nature of the cyDNA produced by these CRCs that underlies the difference in STING activation.⁹ Here, we find that early activation of cGAS/STING in DCs by cyDNA from tumors with different DNA-damaging contexts, such as MSI and IR damage, induce stronger innate and adaptive anti-tumor immunity. We identify differences in cyDNA fragment size, subcellular origin, and repetitive sequences found in these highly stimulatory cyDNAs that explain this improved immune activation and show that they promote anti-tumor immunity in cold CIN tumors. These findings further support the use of STING agonists for neoadjuvant use in anti-tumor immunotherapy and provide the framework for improved design of DNA-based STING agonists.

RESULTS

MSI cyDNA more efficiently activates STING in DCs, leading to improved anti-tumor immunity

Cross-presentation and co-stimulation by DCs is a necessary step for T cell maturation and has been shown to occur as a result of STING activation.²⁰ Interestingly, single-cell RNA sequencing data from orthotopically grown MC38 CRCs that had MSI and CIN because of CRISPR-induced mutations⁹ showed an increased type I IFN-related gene expression set in DCs from MSI tumors (Figures 1A and S1A), possibly a result of damage-associated patterns from the tumor cells. Consistent with this, MSI tumor-infiltrating DCs exhibit higher *Sting* expression compared to DCs in CIN tumors (Figure S1B), and co-culture of bone marrow-derived DCs (BMDCs) with MSI or CIN cells labeled by EdU indicated that DCs were highly capable of taking up tumor-derived DNA from CRC cells (Figure S1C). However, despite improved STING activation in MSI tumors, no differences were observed in cyDNA quantity in MSI and CIN cells.⁹ Therefore, we aimed to determine whether cyDNA in MSI tumors is inherently more stimulatory to the STING pathway than that of CIN CRCs. Stimulation of BMDCs with equal concentrations of cyDNA isolated from MSI and CIN cells showed earlier IFN β and CXCL10 production by MSI cyDNA than CIN cyDNA (Figures 1B and 1C) despite equivalent cyDNA uptake (Figure S1D). This early activation was extinguished by later time points when CIN cyDNA increased IFN β and CXCL10 expression. MSI cyDNA was also more efficient at inducing IFN β and CXCL10 expression than herring testis DNA (HT-DNA), a commonly used STING pathway agonist, confirming that inherent features of the DNA determine its stimulatory capacity. The delay in STING activation by CIN cyDNA was not due to greater overall DNA uptake over longer stimulation time frames, as pulsing BMDCs with MSI or CIN cyDNA for only 15 min did not alter the kinetics of IFN production (Figures S1E and S1F). Therefore, our results indicate that equivalent amounts of MSI cyDNA lead to quicker and earlier activation of the STING pathway in DCs compared to CIN cyDNA.

Next, we wanted to investigate whether early STING activation from MSI cyDNA could improve CD8 $^{+}$ T cell activation, as this is a

key feature of anti-tumor immunity in MSI CRCs.⁷ To do this, ovalbumin (OVA)-pulsed BMDCs were stimulated with equal concentrations of MSI or CIN cyDNA and co-cultured with OVA-specific OT-I CD8 $^{+}$ T cells. Stimulation with MSI cyDNA led to sustained upregulation of the T cell activation markers IFN γ and CD69, as well as the proliferation marker Ki67 (Figures 1D and S1G). To ensure that this finding was not an artifact of the MC38 CRC cell line, we also isolated cyDNA from patient-derived organoid cultures and matched MSI variants in which *MLH1* was knocked down using short hairpin RNA (shRNA).⁹ Consistent with our previous results, stimulation of BMDCs with sh*MLH1* organoid-derived cyDNA upregulated more CD69 on CD8 $^{+}$ T cells compared to cyDNA from matched controls (Figure 1E). Therefore, MSI cyDNA leads to improved T cell activation compared to CIN cyDNA, suggesting that early activation of cGAS/STING in DCs during co-stimulation plays a role in the durable CD8 $^{+}$ T cell-mediated anti-tumor immunity in MSI CRCs.

Our data indicate that cyDNA arising from DNA damage due to genomic instability induces differential STING activation. We therefore questioned whether DNA-damaging therapies would also alter the stimulatory capacity of cyDNA. To investigate this, we first focused on IR, a frequently used DNA-damaging therapy well known to induce STING activation.^{13,16} BMDCs were stimulated with cyDNA isolated 0.5 or 6 h after 10 Gy of IR. Even at equal concentrations, cyDNA from IR-treated cells led to increased TBK1 and STAT1 phosphorylation (Figure S1H), as well as transcription of CXCL10 and IRF7, compared to cyDNA from untreated cells (Figure 1F), regardless of whether the treatment occurred in MSI or CIN cells. We next investigated whether oxaliplatin, a platinum-based DNA-damaging therapy used frequently in CRC as a component of FOLFOX,² could also influence the stimulatory capacity of cyDNA. Consistent with IR treatment, cyDNA isolated from oxaliplatin-treated cells also led to the increased expression of CCL5 and IRF7 upon BMDC stimulation (Figure 1G). Therefore, DNA-damaging treatments can also influence the stimulation potential of cyDNA, with IR and oxaliplatin treatment specifically leading to an increased early stimulatory capacity.

Longer fragments in IR cyDNA lead to increased STING and T cell activation via improved cGAS binding

Previous reports have suggested that longer DNA fragments (>50 bp) are more capable of inducing cGAS activation.²¹ To evaluate the size of cyDNA produced endogenously by MSI or CIN cells, isolated cyDNA was subjected to gel electrophoresis. This indicated that cyDNA in each CRC subtype ranged in size from 10 to 100 bp (Figure S2A). To more sensitively investigate cyDNA size differences, we utilized microfluidics-based electrophoresis with a bioanalyzer (Figures 2A, 2B, S2B, and S2C). Quantification of the resulting curves indicated increased levels of larger cyDNA fragments (>50 bp) following IR treatment, suggesting that DNA damage from IR led to longer DNA fragments being released into the cytosol. No consistent differences in length were observed between cyDNA from MSI and CIN CRCs.

To confirm that increased cyDNA size induced stronger STING activation, scrambled sequence oligos of 30, 50, or 70 bp in length were used to stimulate BMDCs. Consistent

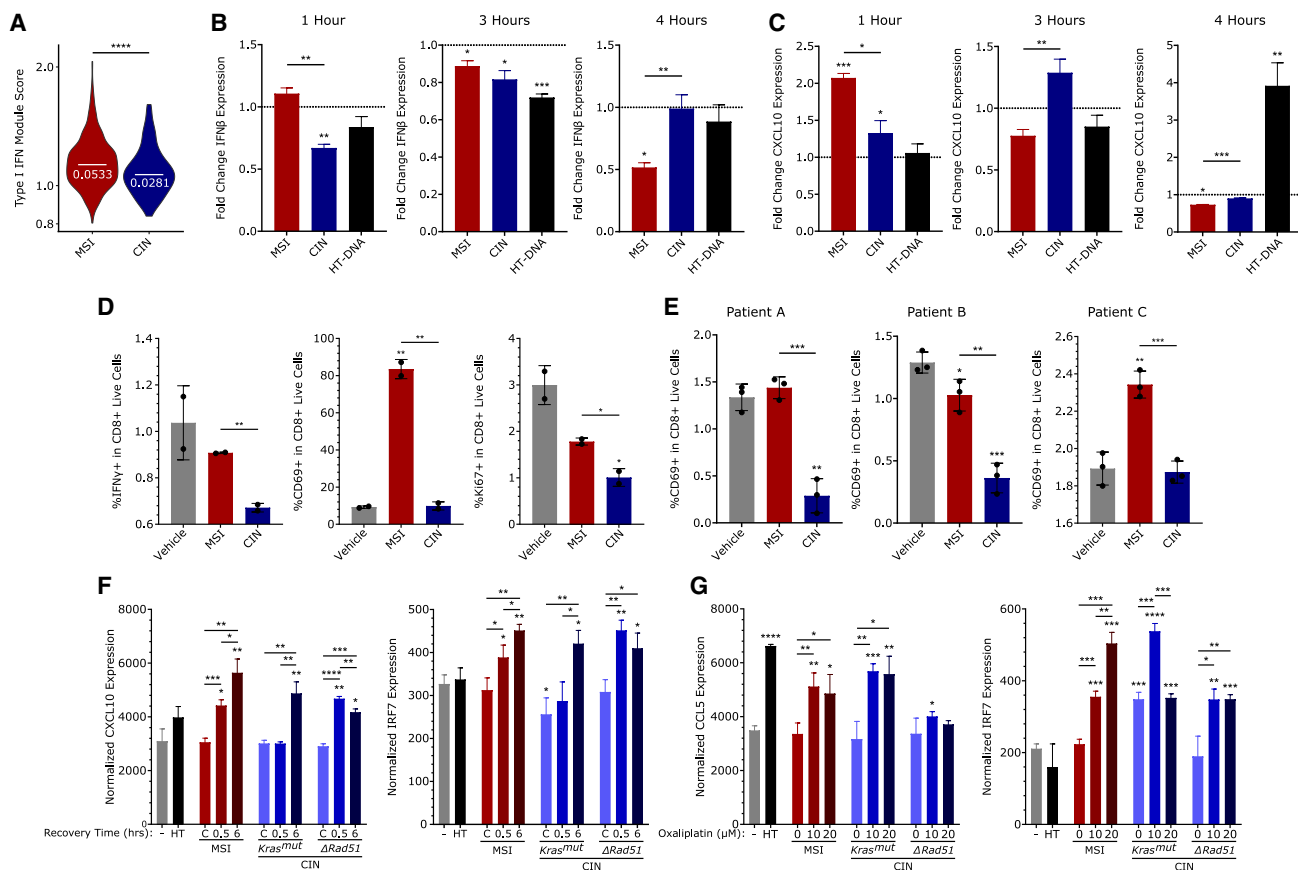


Figure 1. cyDNA from MSI and cells treated with DNA-damaging therapies lead to increased STING signaling in DCs and greater T cell activation

(A) Module score of the type I IFN gene set expression in DCs from orthotopic MSI and CIN (*Kras^{mut}*) CRC tumors analyzed by single-cell RNA sequencing (scRNA-seq).

(B and C) BMDCs were stimulated with cyDNA from MSI and CIN MC38 cells before RNA isolation and qPCR. Data are fold change from lipofectamine control.

(D) BMDCs were stimulated with cyDNA and OVA for 30 min, washed, and co-cultured with OT-I CD8⁺ T cells for 48 h before flow analysis.

(E) OVA-pulsed BMDCs were stimulated with cyDNA from shMLH1 (MSI) or shScramble (CIN) patient organoids for 30 min, washed, and co-cultured with OT-I CD8⁺ T cells for 48 h.

(F) MC38 cells were treated with 10 Gy IR and allowed to recover for 0.5 or 6 h before cyDNA isolation. BMDCs were stimulated with this cyDNA for 30 min, washed, and incubated for 3 h before RNA isolation. – indicates lipofectamine, HT indicates HT-DNA, and C indicates cyDNA from non-IR-treated cells.

(G) MC38 cells were treated with oxaliplatin for 48 h before cyDNA isolation. BMDCs were stimulated with this cyDNA for 30 min, washed, and incubated for a total of 24 h before RNA isolation.

All images show 1 representative replicate of $n = 3$. (D) and (E) are normalized to T cell-only controls. Significance to the lipofectamine control is indicated above the bar, and significance between experimental samples is shown above the connecting lines. * $p < 0.05$, ** $p < 0.01$, *** $p < 0.001$, and **** $p < 0.0001$ (unpaired t test).

with previous reports,²¹ increased levels of pTBK1, pSTAT1, and pSTING were observed with 50 and 70 bp oligos (Figure 2C). To determine whether longer cyDNAs produced endogenously also led to this improved STING activation, MSI cyDNA was separated by size using fast protein liquid chromatography (FPLC) (Figure S2D). BMDC stimulation with longer cyDNAs also led to the increased transcription of IFN α , IFN β , CXCL10, and IRF7 (Figure 2D). To investigate whether DNA of increased size could induce stronger cytotoxic T cell activation, BMDCs stimulated with 30, 70, or 200 bp oligos were co-cultured with CD8⁺ T cells. Analysis of T cell activation by flow cytometry showed the upregulation of IFN γ following stimulation with larger DNAs (Figure 2E). This

indicates that increased cyDNA size not only leads to stronger STING activation but also to more potent cytotoxic T cell activation by DCs.

Next, we wanted to determine whether this increased activation was dependent on canonical cGAS/STING signaling, as other DNA sensors may also stimulate an IFN-mediated response.¹⁰ BMDCs isolated from *Sting^{Gt}* knockout mice stimulated with oligos of different sizes showed strongly decreased expression of CXCL10 and IRF7 compared to wild-type BMDCs (Figure 2F). To examine the role of cGAS specifically, BMDCs were pre-treated with the cGAS inhibitor RU-521²² before stimulation with oligos of different sizes. RU-521 strongly decreased early TBK1 and STAT1 activation from 70 and 200 bp

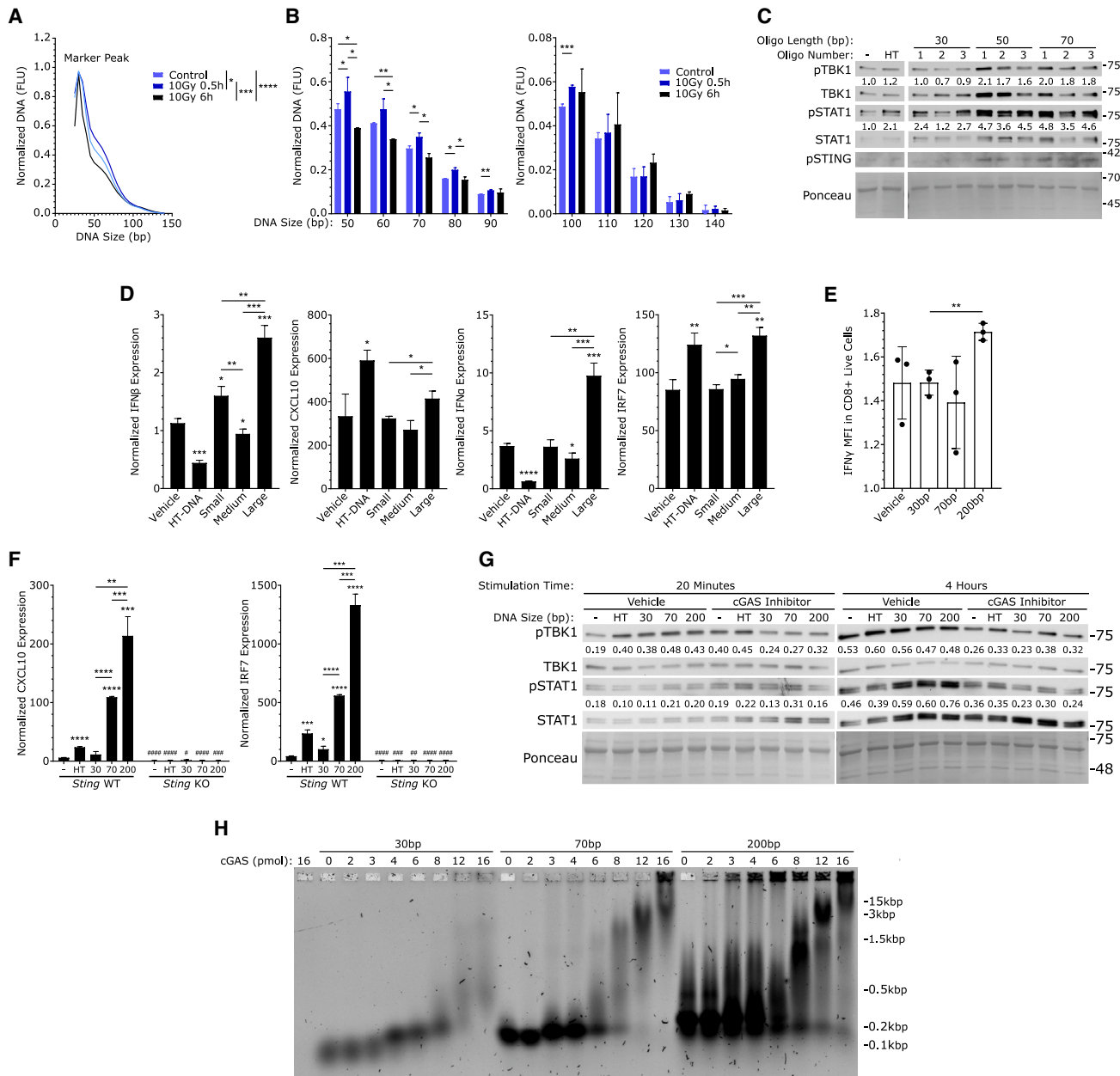


Figure 2. Longer cyDNAs produced by IR treatment induce greater STING pathway activation in DCs

(A and B) Size of cyDNA isolated from IR-treated *Kras^{mut}* CIN cells was determined by bioanalyzer.

(A) Bioanalyzer curves normalized for input concentration to the internal 35 bp kit marker peak. Compiled data of 3 replicates are shown.

(B) Bioanalyzer values normalized to the marker peak at specific sizes. 2 representative replicates are shown of $n = 3$.

(C) BMDCs were stimulated with different scrambled oligos (#1–#3) for 3 h before protein isolation. – indicates lipofectamine, and HT indicates HT-DNA. Quantification is normalized to Ponceau loading control and lipofectamine control.

(D) cyDNA from MSI cells was separated into 3 sizes using FPLC (see Figure S2D) and used to stimulate BMDCs for 3 (IFN β , CXCL10, IFN α) or 4 h (IRF7).

(E) BMDCs were stimulated with oligos (#2 from A) for 30 min, washed, and co-cultured with OT-I CD8 $^{+}$ T cells for 48 h.

(F) Wild-type (WT) or *Sting^{Gl}* knockout (KO) BMDCs were stimulated with oligos (#2 from A) for 24 h. * over the sample bar indicates significance to the lipofectamine control (–), and # over the sample bar indicates significance to WT BMDCs.

(G) BMDCs were pre-treated with RU-521 and stimulated with oligos (#2 from A). Quantification is normalized to Ponceau loading control.

(H) EMSA of cGAS binding to DNA oligos (#2 from A).

All data show representative replicates from $n = 3$ experiments. Significance to lipofectamine control is indicated above the sample bar. * or # $p < 0.05$, ** or ## $p < 0.01$, *** or ### $p < 0.001$, **** or #### $p < 0.0001$ (two-way ANOVA: A, paired t test; B, or unpaired t test: C–H).

oligo stimulation (Figure 2G). To determine the underlying mechanism, we then evaluated whether larger cyDNAs exhibited improved binding to cGAS using an electrophoretic mobility shift assay (EMSA), where increased binding is indicated by the reduced migration of the complex through an agarose gel. We observed binding of the 70 and 200 bp oligos at lower cGAS concentrations than 30 bp DNA (Figures 2H and S2E). Consistent with this, increased cGAS oligomerization, which occurs as cGAS binds to cyDNA,¹¹ was also observed with the 70 and 200 bp DNAs (Figure S2F). Taken altogether, these data suggest that longer cyDNA fragments, such as those produced by IR treatment, lead to stronger cGAS/STING activation in DCs and, thereby, stronger T cell activation.

cyDNA in CRC cells is enriched for specific genetic elements

To begin characterizing cyDNA from MSI vs. CIN cells and identifying the differences that underlie the improved STING activation by cyDNA from MSI CRCs and CRCs treated with DNA-damaging therapy, we performed next-generation sequencing on cyDNA from MSI and CIN cells treated or not with IR or 5-fluorouracil (5-FU). 5-FU is a common treatment for CRC in both FOL-FOX and FOL-FIRI combination therapies and induces DNA damage through the integration of modified bases and nucleotide imbalance.^{2,23} First, we sought to characterize the overall composition of cyDNA in all samples to understand the nature of cyDNA in general. Although cyDNA mapped to sequences from each chromosome, we observed an unexpectedly high amount of reads from chromosomes 2, 9, 11, and 15 upon comparison to the expected percentage of each chromosome in cyDNA based on base-pair size (Figure 3A). This was combined with unexpectedly low cyDNA contributions from chromosomes 3, 4, 6, 14, 16, 18, and X. cyDNA was also enriched in reads mapping to protein-coding gene areas, including both exons and introns (Figures 3B and 3C), suggesting selection for euchromatic regions of the genome. Surprisingly, when examining which genes CRC cyDNA mapped to, we observed that 2 of the 5 most common genes across our samples were the immunoglobulin genes *Igk* and *Igh*, which were present in 19.4% and 16.1% of cyDNA samples, respectively (Figure 3D). This bias for certain chromosomes and genes within cyDNA indicates that its composition is not random and suggests that there is more DNA damage at these sites overall or that DNA fragments may be exported to the cytosol by a specific and selective mechanism.

Many recent studies have investigated how mitochondrial DNA (mtDNA) release into the cytosol induces STING activation.^{24,25} We found an overall low amount of mtDNA in the cytosol, comprising an average of 0.08% of cyDNA in CRC cells (Figure 3E). Another aspect of cyDNA under intense investigation is retrotransposons, such as LINEs and SINEs, which have been shown to play a role in STING activation during senescence, aging, and cancer.^{26,27} To evaluate the levels of transposons and other repetitive regions in cyDNA, we examined reads that mapped to regions annotated by RepeatMasker, which identifies repetitive and low complexity regions within the genome, including LINEs, SINEs, and satellites.²⁸ Using this tool, we found that an average of 13.5% of cyDNA mapped to repetitive regions of the

genome (Figure 3F), with the largest contributor being LINEs, long terminal repeats (LTRs), and satellites (Figure 3G). Altogether, these data indicate that there are specific mechanisms underlying the composition of cyDNA.

Genomic instability from MSI and IR produce specific sequence and motif changes within cyDNA

To identify patterns prevalent in highly stimulatory cyDNAs, we investigated our sequencing data for differences between MSI and CIN cyDNA or cyDNA from IR-treated or untreated cells. Although mtDNA was a small fraction of cyDNA content (Figure 3E), we observed a trend toward increased mtDNA in the cytosol 6 h after IR treatment (Figure 4A). In contrast, cyDNA isolated from 5-FU-treated cells showed no difference in mtDNA content (Figure S3A). This suggests that IR, but not all DNA-damaging agents, promotes the release of mtDNA into the cytosol.

MSI cancers are characterized by point mutations and frame-shifts resulting from polymerase slippage, most evident within microsatellite regions,⁵ suggesting that DNA from damaged microsatellite regions could be more prevalent in the cytosol in these cells. We therefore examined the repetitive patterns of cyDNA in our sequencing data using RepeatMasker annotated regions. We observed differences in the levels of “other” and SINE annotated regions in MSI and CIN cyDNA that is MSI and CIN (Figure S3B). However, no differences were observed in satellite or simple repeat (microsatellite) levels (Figure S3C). We then considered the possibility that highly repetitive regions are well known to be difficult to accurately map and often require long sequencing reads to do so, which would not be possible in short, fragmented cyDNA. Therefore, we performed sequenced-based analysis on all cyDNA sequencing reads, regardless of whether or not they mapped to the mouse genome, using MicRocounter,²⁹ a Bioconductor package that identifies 2–6 bp microsatellites in raw sequence data. This revealed increased microsatellite content in MSI cyDNA compared to CIN cyDNA (Figure 4B). Additionally, microsatellites found in MSI cyDNA were of longer lengths. Similar results were found with single-base-pair microsatellites (Figure 4C). Lower GC content in MSI cyDNA was also observed (Figure S3D). Therefore, MSI leads to cyDNA with increased microsatellite repeats.

Surprisingly, increased microsatellites were also observed in the cytosol of all CRCs 6 h after IR treatment (Figure 4D) but not after treatment with 5-FU (Figure S3E). Consistent with this, decreased sequence complexity was also observed (Figure S3F), which is indicative of repetitive sequences. IR and 5-FU both led to changes in cyDNA GC content (Figure S3G). Interestingly, RepeatMasker analysis of IR-induced cyDNA also suggested increased levels of DNA transposons in the cytosol after 0.5 h, which was largely due to the Charlie-hAT transposon type (Figures S3H and S3I). To our knowledge, DNA transposons, a type of transposon that translocates via a double-stranded DNA intermediate,³⁰ have not yet been reported within cyDNA. Additionally, the mechanism for their presence in cyDNA is not as clear as for retrotransposons since DNA transposons are traditionally considered fossils and therefore thought to be no longer capable of translocation in most mammals.^{30,31} Given that Charlie-hAT is

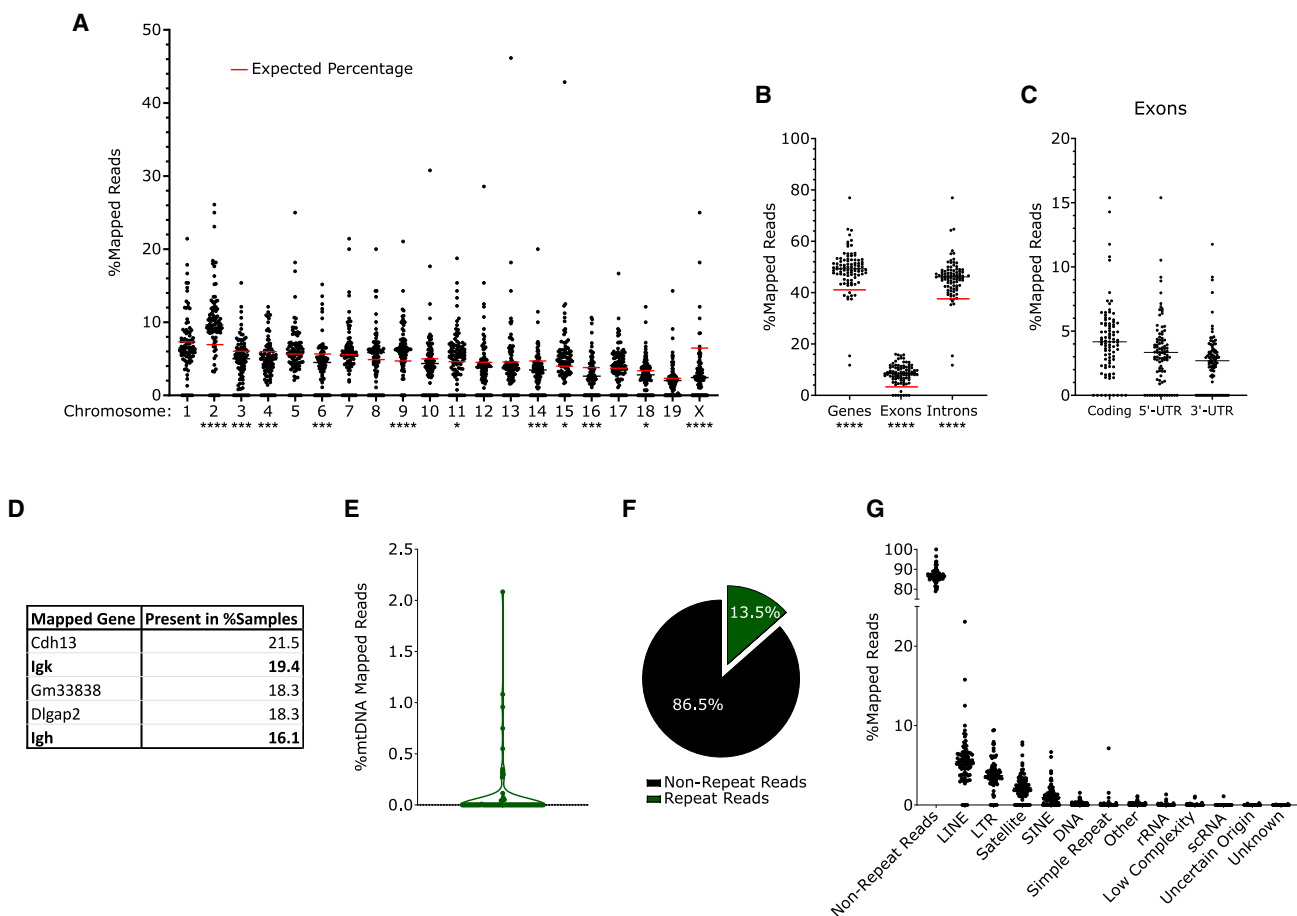


Figure 3. cyDNA contains chromosomal, mitochondrial, and repetitive DNA sequences

cyDNA from cells with MSI and CIN treated or not with 10 Gy IR (see Figure 1F) or 5-FU (1.0 or 1.5 μ M) for 24 h was sequenced.

(A) Percentage of cyDNA from the indicated chromosome. Red line indicates the expected cyDNA contribution.

(B and C) Percentage of cyDNA mapped to gene coding regions (B) or exon regions (C). Red line indicates the expected percentage of protein-coding genes in cyDNA at random.

(D) Top 5 most common genes across all cyDNA samples.

(E) Percentage of reads mapped to mitochondria.

(F and G) RepeatMasker analysis of repetitive regions (F) and average cyDNA contribution (G) per sample.

* $p < 0.05$, ** $p < 0.001$, and *** $p < 0.0001$ (one-sample t test vs. expected, A and B, indicated under the x-axis).

the most common DNA transposon in humans,³¹ understanding the presence of DNA transposons within cyDNA, particularly following IR treatment, could be important in the future for understanding immune responses from IR in patients with CRC.

Cytosolic mtDNA is more stimulatory than cytosolic genomic DNA

Our finding of increased mtDNA in the cytosol following IR (Figure 4A) was intriguing, as the microbial origin of the mitochondria³² leads to unique mtDNA properties that may improve sensing by cGAS, which evolved to sense microbial DNA as non-self. We thus sought to investigate the role of increased mtDNA in the cytosol in cGAS/STING activation. First, to confirm the trend observed in our sequencing data (Figure 4A), MSI and CIN cyDNA was isolated following 10 Gy of IR treatment and analyzed by qPCR using mtDNA specific primers. At 6 h after

IR treatment, mtDNA made up a greater proportion of total cyDNA compared to untreated controls, specifically in MSI cells (Figure 5A). To determine whether this increased mtDNA content led to differential cGAS/STING activation, MSI cells were treated with ethidium bromide (EtBr) for 7 days before cyDNA isolation. EtBr has been used extensively in the literature to specifically deplete mtDNA due to its accumulation within the mitochondria and intercalation into highly replicating mtDNA, preventing its replication.³³ After confirming that cyDNA from EtBr-treated cells was depleted of mtDNA (Figure S4A), BMDCs were stimulated with equal concentrations of cyDNA from mtDNA-depleted or control MSI cells. mtDNA-depleted cyDNA induced drastically lower levels of IFN β and IFN α (Figure 5B), indicating that cytosolic mtDNA is a potent inducer of STING. To understand the relative stimulatory capacity of cytosolic mtDNA compared to genomic DNA, BMDCs were stimulated with differing ratios of

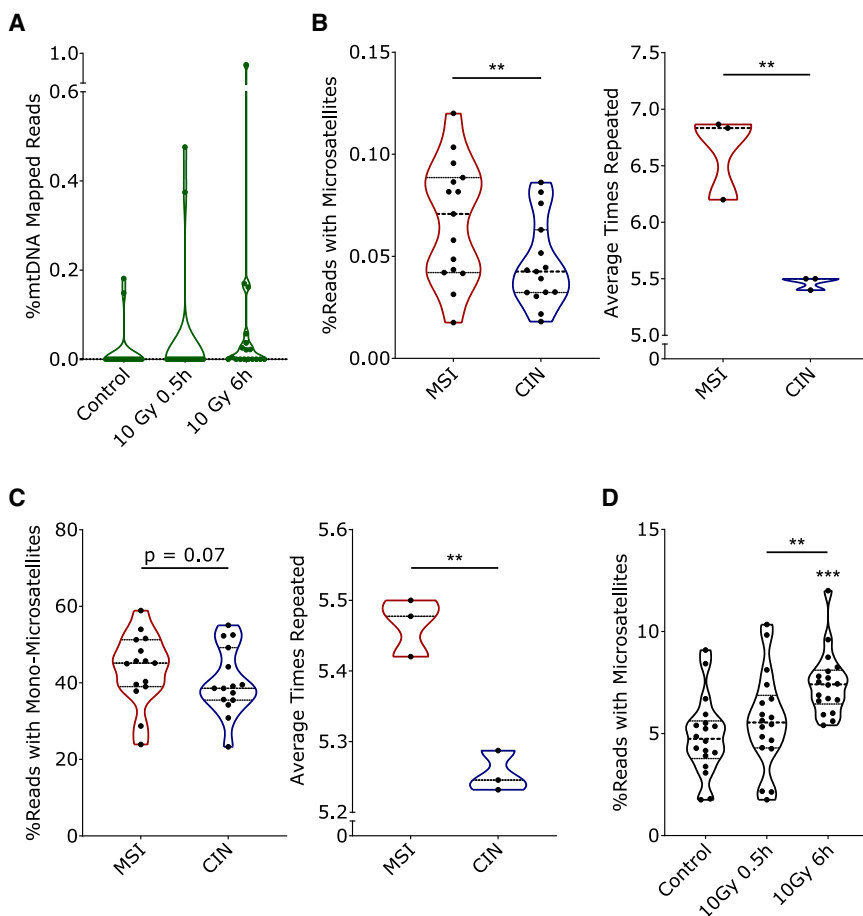


Figure 4. Strongly stimulatory cyDNAs contain higher levels of mtDNA and microsatellites

(A) Percent of IR-treated cyDNA sequencing reads mapping to mitochondria (see Figure 1F) in all CRC subtypes.

(B) Left: percentage of all mapped and unmapped reads that contain >5 2–6 bp microsatellite repeats for all treatments combined. Right: average number of times sequence is repeated in untreated cells.

(C) Left: percentage of reads with >5 1 bp microsatellite repeats from all treatments combined. Right: average number of times each repeat was repeated in untreated cells.

(D) Percentage of all mapped and unmapped reads that contain >5 2–6 bp microsatellite repeats after 10 Gy IR (see Figure 1F) from all CRC subtypes combined.

All sequencing was performed with 3 biological replicates, and pooled data are shown. Significance to the untreated control is indicated over the sample bar (D). ** $p < 0.01$ and *** $p < 0.001$ (paired t test: B, left, C, left, and D; unpaired t test: B, right, and C, right).

mtDNA to genomic DNA isolated from MSI cells and sonicated to equivalent sizes (Figure S4B). Increased ratios of mtDNA led to higher expression of IFN β and IRF7 (Figure 5C), confirming that improved STING activation by cytosolic mtDNA was not an artifact of EtBr use. Interestingly, no consistent differences were observed with mtDNA from CIN cells. Taken together, these data indicate that MSI mtDNA is more stimulatory to cGAS/STING than genomic DNA, which may provide an explanation for the improved stimulatory capacity of MSI cyDNA from IR treatment in CRCs. Further investigation will be required to determine what aspects of mtDNA, such as structure, methylation differences, or increased oxidative damage,^{34–36} drive this improved immune stimulation.

Microsatellites in MSI cyDNA lead to improved STING activation through cGAS

Sequencing analysis of MSI and CIN cyDNA indicated that more stimulatory MSI cyDNA contained higher levels of microsatellites (Figures 4B and 4C), a result that is consistent with the high levels of DNA damage and mutation within microsatellite regions of MSI cells.⁵ To determine whether microsatellites specifically lead to increased STING activation, BMDCs were stimulated with 200 bp oligos containing a scrambled sequence or the sequence of a microsatellite-containing read identified in our cyDNA sequencing data. As our sequencing data contained reads

with microsatellites positioned both in the middle of the cyDNA fragment and on the edge, we positioned the microsatellites in each of these locations in our oligos to determine if this was important to STING activation. Both edge and middle microsatellite oligos led to increased phosphorylation of TBK1 and STING

(Figure 6A) and increased CXCL10 and IRF7 expression (Figure 6B) compared to scramble controls, confirming their increased stimulatory capacity. To determine whether endogenous microsatellite-containing cyDNA also increased STING activation, we isolated microsatellite-containing cyDNA from total MSI cyDNA using a sequence-specific pull-down with probes containing microsatellite motifs found to be enriched in our sequencing data (Figures 6C and S5A). Stimulation of BMDCs with equal concentrations of this microsatellite-enriched cyDNA showed increased pTBK1, pSTAT1, and pNF- κ B from microsatellite-rich cyDNA compared to pull-down controls (Figure 6D). To examine whether microsatellites could induce the improved T cell activity observed with MSI cyDNA (Figures 1D and 1E), BMDCs stimulated with microsatellite- or scrambled-sequence-containing oligos were co-cultured with CD8 $^+$ T cells. Microsatellite-containing oligos induced increased levels of Ki67 $^+$ T cells (Figure 6E), indicating increased and sustained T cell proliferation. Therefore, increased microsatellites in MSI cyDNA lead to improved cGAS/STING activation and cytotoxic T cell activity.

Next, we wanted to investigate whether the improved stimulatory capacity of microsatellite cyDNA was dependent on canonical cGAS/STING signaling or influenced by other cyDNA-sensing PRRs. *Sting*^{Gt} knockout BMDCs showed a completely diminished response to stimulation with microsatellite oligos compared to

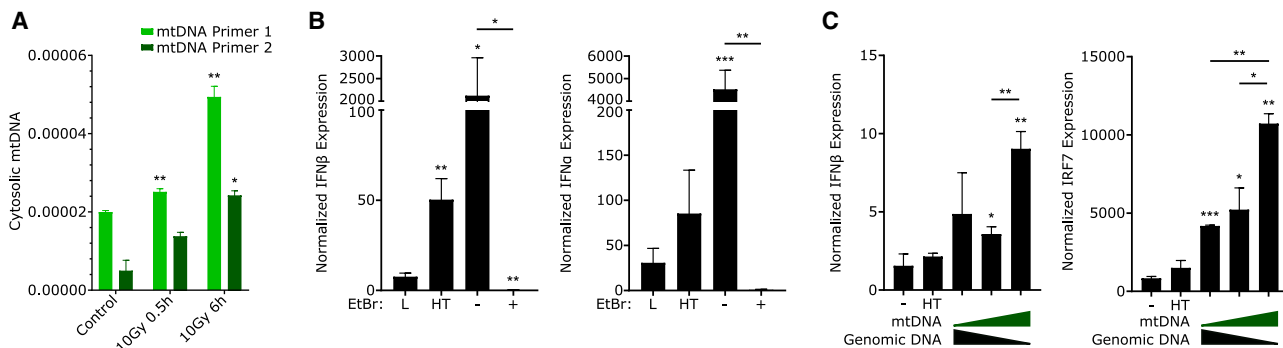


Figure 5. Cytosolic mtDNA induces stronger STING activation in DCs than cytosolic genomic DNA

(A) mtDNA-specific sequences in cydDNA from MSI cells treated with 10 Gy IR (see Figure 1F) were quantified using qPCR and normalized to total cydDNA quantity. (B) BMDCs were stimulated for 24 h with cydDNA isolated from MSI cells treated with EtBr for 7 days to deplete mtDNA. L indicates lipofectamine control, and HT indicates HT-DNA.

(C) mtDNA and genomic DNA were isolated from MSI cells and sonicated to equal size. BMDCs were stimulated with mtDNA, genomic DNA, or a 50:50 mix of both for 1 (IFN β) or 4 (IRF7) hours. – indicates lipofectamine control.

All data show representative replicates from $n = 3$ experiments. Significance to unirradiated control (A) or lipofectamine control (B and C) is indicated over the sample bar. * $p < 0.05$, ** $p < 0.01$, and *** $p < 0.001$ (unpaired t test).

wild-type BMDC controls (Figure 6F). Likewise, stimulation of BMDCs pre-treated with the cGAS inhibitor RU-521 with microsatellite oligos decreased their levels of pTBK1, pSTAT1, and pSTING compared to vehicle controls (Figure 6G), suggesting that microsatellites lead to improved cydDNA sensing by cGAS, thereby inducing STING activation. Consistent with this, BMDC stimulation and protein isolation under non-denaturing conditions indicated increased cGAS oligomerization by microsatellite sequences (Figure S5B). To determine whether this increased cGAS activation was due to improved binding to cGAS by microsatellites, BMDCs were competitively co-stimulated with equal concentrations of scrambled and microsatellite-containing oligos before pull down of cGAS and qPCR to examine bound oligo levels. Both edge and middle oligos were more frequently bound to cGAS compared to the scrambled control (Figure 6H). In contrast, pre-treatment with IN-3, an inhibitor of the PRRs AIM2 and NLRP3, which also respond to cydDNA,^{10,34,37} led to earlier phosphorylation of TBK1, STAT1, and STING from microsatellite-containing oligos (Figure S5C), suggesting possible competition for microsatellites in the cytosol between these sensors. Altogether, these data indicate that microsatellites are an important contributor to the increased stimulatory capacity and anti-tumor immunity of MSI cydDNA through greater STING activation and T cell activation by increased binding to cGAS.

Microsatellite cydDNA induces improved DC and T cell activation in cold CIN tumors

Finally, we wanted to investigate whether increased STING and T cell activation from microsatellite-activated DCs could improve anti-tumor immune responses in CIN tumors, whose cold immunosuppressive microenvironment typically drives poor responses to immunotherapies such as checkpoint inhibition.³⁸ To do this, BMDCs were stimulated with oligos of 200 bp in size containing scrambled or microsatellite sequences. Following these stimulations, BMDCs were adoptively transferred by intraperitoneal injec-

tion into immunocompetent mice bearing orthotopically implanted CIN tumors in the colon (Figure 7A). After 2 weeks, the tumors were collected, and flow cytometry was used to evaluate the anti-tumor immune response (Figure S6). The transfer of microsatellite oligo-stimulated DCs led to increased activation of endogenous type I (CD103^{Hi}) and type II (CD11b^{Hi}CD103^{Mid}) DCs³⁹ in the tumor (Figure 7B), but not the mesenteric lymph nodes (MLNs) or spleen, despite CFSE⁺-transferred DCs homing largely to the MLN and spleen (Figures S7A–S7C). This increase was strongest for DCs stimulated with the middle microsatellite oligo and was matched by increased CD8⁺ T cell infiltration and activation in the tumors, as shown by the T cell activation markers CD69 and IFN γ (Figures 7C, S7D, and S7E). No differences were observed in CD4⁺ regulatory T (Treg) or Thelper cells, natural killer (NK) cells, or macrophages, further highlighting the specificity of the STING-DC-CD8⁺ T cell axis (Figures S7F–S7I). Notably, these trends were observed with transferred BMDCs expressing equivalent levels of STING, suggesting that microsatellite cydDNA may be the initiator of MSI anti-tumor immunity (Figure S1B). One concern for the clinical use of STING agonists is that the upregulation of PD-L1 can occur as a result of increased type I IFN production.¹³ However, no increase was observed in PD-L1 expression on CD45[−] tumor cells upon adoptive transfer of microsatellite-stimulated DCs (Figure S7J). This suggests that microsatellite cydDNA can be formulated in a way that leads to improved T cell activation and infiltration in cold CIN tumors without inducing undesirable, systemic side effects. Such an adjuvant treatment could thus help sensitize CIN tumors to other immunotherapy treatments, leading to improved prognoses for patients with CIN CRCs.

DISCUSSION

Uncovering the mechanisms underlying successful anti-tumor immunity in MSI CRCs provides the opportunity to identify novel treatment strategies that are effective in immunologically cold

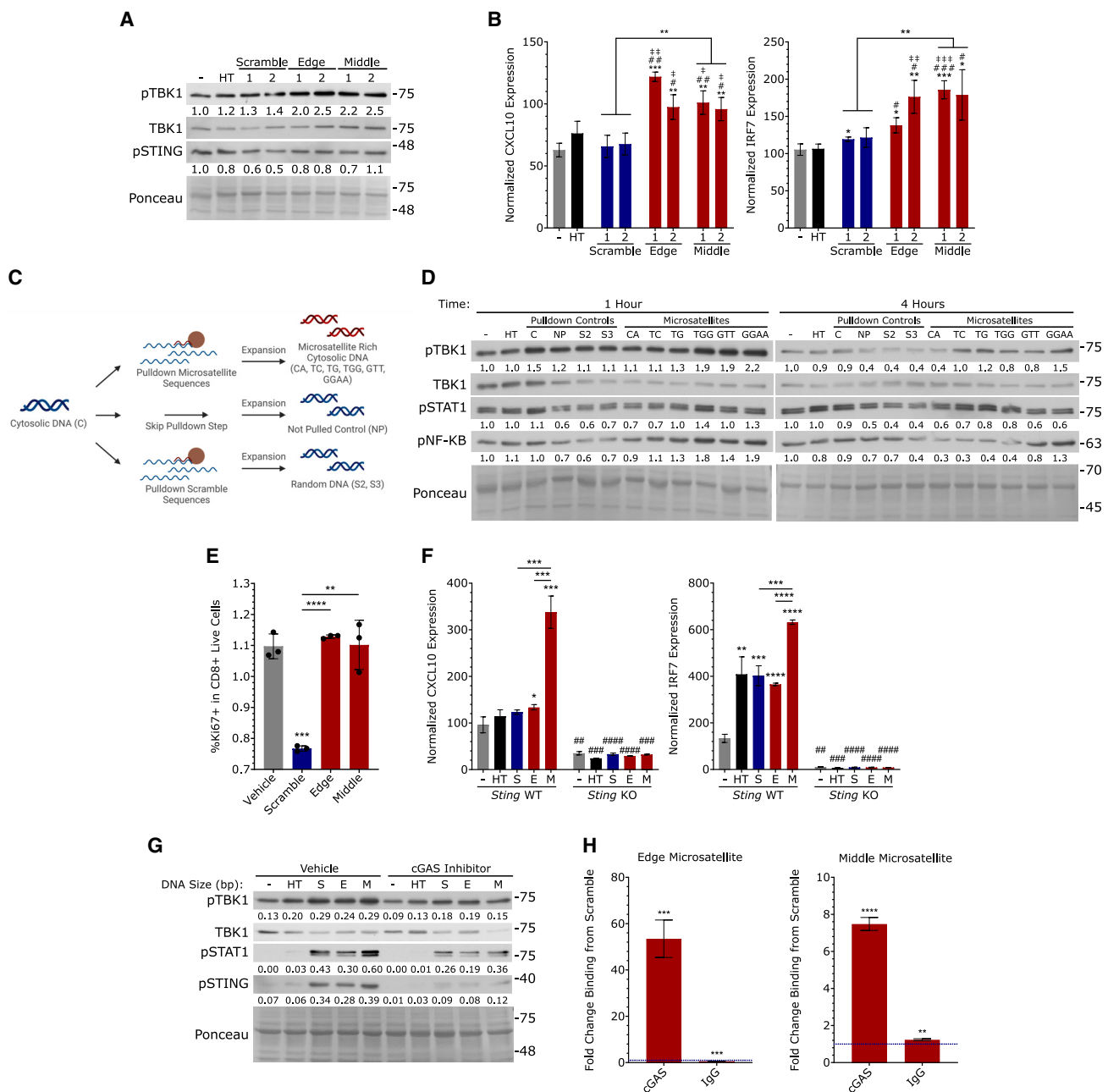


Figure 6. Microsatellite-rich cyDNA in MSI CRCs induce stronger STING and T cell activation by DCs

(A and B) BMDCs were stimulated with oligos containing scrambled or microsatellite sequences at the edge or middle of the oligo before analysis by western blot (A) and qPCR (B). Blot quantifications are normalized to the Ponceau loading control and lipofectamine control. * indicates statistical significance to lipofectamine control, # indicates significance to scramble oligo 1, and + indicates significance to scramble oligo 2. Significance between oligo pairs is indicated with * above the connecting bars.

(C) Schematic of microsatellite pull-down using microsatellite-specific or scrambled probes for isolation of microsatellite-rich cyDNAs from cancer cells (see Figure S5A).

(D) Microsatellites were pulled down from MSI cyDNA and used to stimulate BMDCs. – indicates lipofectamine control; HT indicates HT-DNA; C indicates unmanipulated cyDNA; NP indicates the non-pulled control that skipped the pull-down step but received all other manipulations; S2 and S3 indicate pull-downs with scramble probes; and CA, TC, TG, TGG, GTT, and GGAA indicate microsatellites pulled down. Quantifications are normalized to Ponceau loading control and lipofectamine control.

(E) Oligos containing microsatellite or scrambled sequences (#2 from A) were used to stimulate BMDCs for 30 min before washing and addition of OT-I CD8⁺ T cells for 24 h before flow analysis. Data were normalized to T cell-only controls.

(legend continued on next page)

tumors. One such neoantigen-independent mechanism is activation of cGAS/STING and type I IFN signaling pathways, which we have previously shown are important for anti-tumor immunity in MSI CRC.⁹ However, our previous work and that of others did not identify the underlying mechanism for the activation of these pathways in MSI CRCs. Here, we have identified the specific stimulatory features of cyDNA in MSI CRCs that activate these pathways and further show that this can be replicated using DNA-damaging radio- and chemotherapies. Specifically, we observed enrichment of sequence patterns in cyDNA from genetically unstable tumors that leads to highly potent activation of cGAS/STING. These patterns include microsatellites in MSI cyDNA that we show increase cGAS binding and STING pathway activation in DCs and translate to improved T cell-mediated anti-tumor immunity in CIN CRCs *in vivo*. We further show that the induction of DNA damage by IR treatment leads to larger cyDNA fragment sizes and increased mtDNA leakage into the cytosol, both of which potently increase STING and T cell activation. Notably, we have also identified DCs in the tumor microenvironment as key drivers of cGAS/STING-mediated anti-tumor immunity in MSI CRCs in response to tumor-derived cyDNA.

We are not the first to identify STING as a key player in converting immunosuppressive cold tumors to hot tumors, and STING agonists are currently in clinical trials in combination with checkpoint inhibition therapies.¹⁷ Indeed, Guan et al.⁴⁰ observed that cyDNA production in MSI cancers could occur from hyperexcision of DNA by EXO1 due to a loss of MLH1 expression. Further evaluation will be needed to determine if EXO1 plays a role in the increased microsatellite presence in MSI CRC cyDNA. A recent study by Wang et al.⁴¹ also identified STING activation in type I DCs, but not tumor cells, as necessary for effective CD8⁺ T cell-mediated tumor rejection by STING agonists, consistent with our finding of DC-mediated anti-tumor immunity resulting from MSI cyDNA. Our work also confirms previous findings in the literature that DNA fragment sizes >50 bp led to improved cGAS activation.²¹ This is thought to be due to the improved ability of cGAS to oligomerize, and therefore produce 2'3'-cGAMP, on longer DNA strands.⁴² Additionally, we determined that endogenous cyDNA contains different sizes, that treatments like IR can increase the proportion of large cyDNA fragments, and that microsatellite-containing cyDNAs are especially stimulatory. Our work can thus serve as a foundation for improving the design of STING-agonist-based neoadjuvant therapies.

We performed next-generation sequencing on cyDNA from cancer cells with different sources of genomic instability and DNA damage to characterize the resulting changes in composition. To our knowledge, we are the first to sequence cyDNA in this manner. This sequencing-based screen was chosen due

to the sequence-specific nature of MSI-associated damage and therefore, we suspected, its resulting cyDNA. This strategy allowed us to identify microsatellites as being more prevalent in MSI cyDNA and having a greater ability to induce STING activation through stronger cGAS binding, leading to overall improved anti-tumor immunity. This sequence-dependent mechanism contradicts the current dogma of cGAS as a sequence-independent cyDNA sensor.¹⁰ One possibility is that microsatellite sequences could form secondary DNA structures that improve cGAS binding and oligomerization around the structured cyDNA strand. Consistent with this, Herzner et al.⁴³ found that DNAs as small as 12 bp were capable of inducing strong IFN induction with the addition of Y-form ends. However, our pull-down of microsatellites from the cyDNA of MSI cells for stimulation utilized PCR to expand cyDNA quantities and re-form the double-stranded composition of cyDNA, leading to a linear final product. This suggests that microsatellites can improve STING activation without the formation of secondary DNA structures. Other sources have also identified sequence-dependent variations in STING activation. Herzner et al.⁴³ observed that activation by small Y-form DNA required guanosine ends, while Gentili et al.⁴⁴ found improved IFN production from AATGG centromeric repeats at DNA sizes of 20–30 bp. These data suggest that the traditional sequence-independent view of cGAS may not be absolute and requires further study.

Overall, our work identifies novel patterns of cyDNA composition arising from different forms of genomic instability that activate STING in DCs and lead to improved T cell infiltration and activation. This appears to be a central mechanism underlying the superior anti-tumor immunity observed in MSI CRC. Moving forward, these findings will enable the improved design of DNA-based STING agonists as a neoantigen-independent immunotherapy and set the stage for further analysis of how such agonists can be crafted to maximally activate STING-mediated anti-tumor immunity without also triggering tumor-promoting inflammation.

Limitations of the study

One limitation of our study was the inability to provide tumor growth measurements for our *in vivo* experiments, which were conducted with orthotopically implanted CRC tumors in the colon. No consistent differences were observed in tumor size at endpoint, and although tumor growth evaluation through the course of these experiments would be heavily desirable, the position of the tumor in close proximity to the bladder leads to important anatomical limits for using any kind of tracer-based imaging modality, such as positron emission tomography (PET). However, this limitation is outweighed by the significant

(F) Wild-type (WT) and *Sting*^{Gt} knockout (KO) BMDCs were stimulated with microsatellite or scrambled sequence oligos (#2 from A) for 3 (CXCL10) or 24 h (IRF7). S indicates scrambled oligo, E indicates the edge microsatellite oligo, and M indicates the middle microsatellite oligo. * above the sample bar indicates significance to lipofectamine control (−), and # indicates significance to WT BMDCs.

(G) BMDCs were pre-treated with RU-521 before stimulation with scrambled or microsatellite oligos (#2 from A) for 3 h. Quantifications were normalized to Ponceau loading control.

(H) BMDCs were co-stimulated with 2 µg each of scrambled and edge microsatellite oligos or scrambled and middle microsatellite oligos (#2 from A) for 40 min followed by isolation of the cytosolic fraction and chromatin immunoprecipitation (ChIP)-qPCR for cGAS. CTs were normalized to total oligo amount in the cytosol (non-pulled whole-cytosolic control) and are shown as the fold change of microsatellite oligo from scramble oligo.

All data show representative replicates from $n = 3$ experiments. *, #, or $\#p < 0.05$; **, ##, or $\#\#p < 0.01$; ***, ###, or $\#\#\#p < 0.001$; and ****, #####, or $\#\#\#\#p < 0.0001$ (unpaired t test).

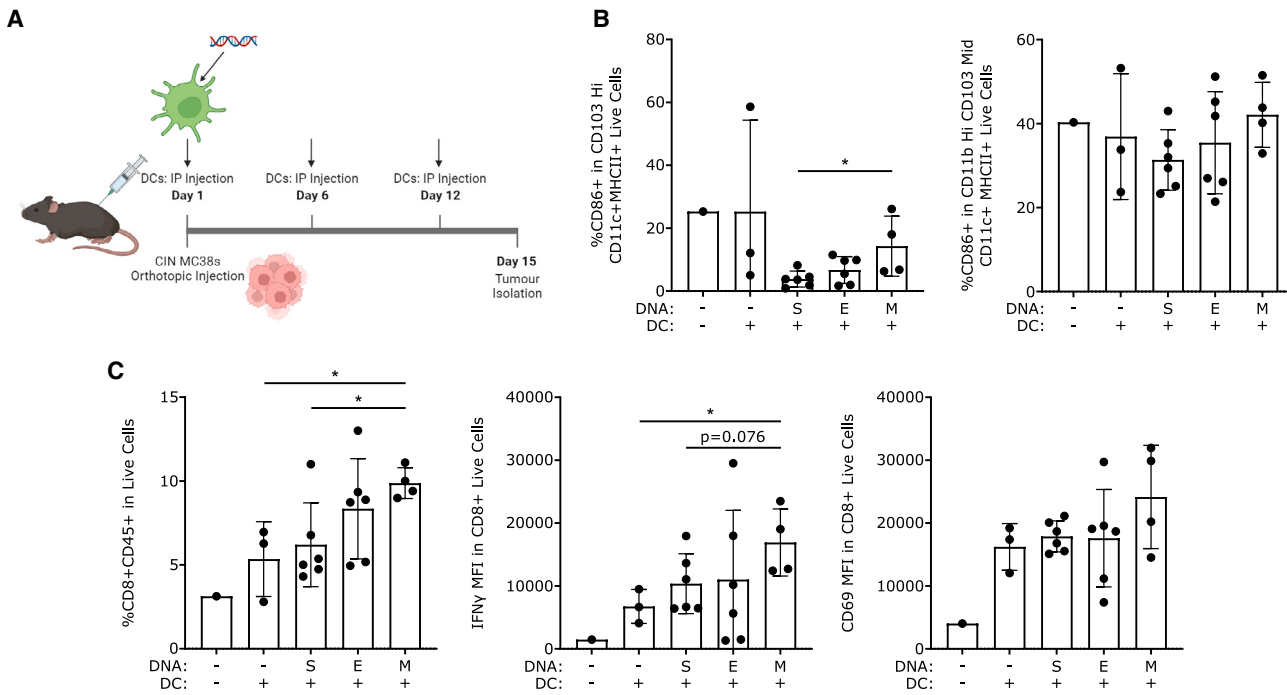


Figure 7. DC activation by microsatellite-rich cyDNA leads to improved anti-tumor immunity

(A) CFSE-stained BMDCs were stimulated with 200 bp DNA oligos containing scrambled or microsatellite sequences (oligo set 2) for 30 min before intraperitoneal injection into orthotopic CIN tumor-bearing mice as indicated.

(B and C) Tumors were isolated and evaluated for type I (B, left) and type II DC activation (B, right) and CD8⁺ T cell infiltration and activation (C) by flow cytometry. S indicates scrambled sequence, E indicates the edge microsatellite oligo, and M indicates the middle microsatellite oligo. 2–6 mice per experimental group. Data show representative replicate from $n = 3$ experiments. * $p < 0.05$ (unpaired t test).

benefits of an orthotopic model that accurately replicates the natural tumor microenvironment and physiological conditions in the intestine in a way that cannot be achieved in subcutaneous tumors.^{45–47} While the orthotopic model achieved our aim of demonstrating the therapeutic potential of using microsatellite-rich cyDNA to increase anti-tumor immunity in the physiological context of CRC, clinical translation of this work will require additional model systems to optimize treatment formulation and neoadjuvant pairings that decrease overall tumor growth. An additional limitation of our work is that our sequencing method did not capture the many other variations within cyDNA that are likely present, such as chemical modifications, methylation, structure, and histone modifications. Indeed, a study by Balzarolo et al.⁴⁸ showed increased IFN β expression and DC activation upon stimulation using m6A-methylated DNA oligos compared to unmethylated controls. This modification is rare in mouse and humans but common in prokaryotes. As m6A is enriched in mtDNA,³⁵ this finding may have important implications for the increased STING activation by cytosolic mtDNA. An additional limitation is that this study focused on analysis of free, fragmented cyDNA, and the role of cyDNA arising from micronuclei was not investigated. Interestingly, a recent study by MacDonald et al.⁴⁹ found the histone marker H3K79me2 in micronuclei led to increased cGAS co-localization and IFN-stimulated gene expression, suggesting that histone modifications and protein-based differences in micronuclei may affect the level of STING activation.

RESOURCE AVAILABILITY

Lead contact

Further information and requests for resources and reagents should be directed to and will be fulfilled by the lead contact, Kristi Baker (kbaker@ualberta.ca).

Materials availability

This study did not generate new unique reagents.

Data and code availability

- cyDNA sequencing data have been deposited at NCBI Sequence Read Archive and are publicly available as of the date of publication. Accession numbers are listed in the [key resources table](#).
- This paper does not report original code.
- Any additional information required to reanalyze the data reported in this work paper is available from the [lead contact](#) upon request.

ACKNOWLEDGMENTS

The authors thank Dan McGinn, Cheryl Santos, Daming Li, Sudip Subedi, Jessica Hamilton, Dr. Xuejun Sun, Dr. Anne Galloway, and Dr. Lei Li, as well as the Advanced Cell Exploration core at the University of Alberta, for technical support. Dr. Avalyn Stanislaus and Dr. Michael Sawyer provided experimental support and advice. Patient samples for organoid development were provided by Dr. Daniel Schiller and Rose-Marie Corrand. This project was supported by funding from the Canadian Institutes of Health Research (grant 407882) (K.B.), the Natural Sciences and Engineering Research Council of Canada (grant RGPIN-2016-05152) (K.B.), the Canadian Foundation for Innovation (K.B.), and the University Hospital Foundation (K.B.).

AUTHOR CONTRIBUTIONS

Conceptualization, S.R.M. and K.B.; methodology, S.R.M., A.C., F.M.-S., V.M.-S., and K.B.; investigation, S.R.M., A.C., D.N.W.D., S.C., and C.M.; writing – original draft, S.R.M. and K.B.; writing – review & editing, S.R.M., A.C., C.M., F.M.-S., V.M.-S., and K.B.; funding acquisition, K.B.; resources, F.M.-S. and V.M.-S.; supervision, K.B.

DECLARATION OF INTERESTS

The authors declare no competing interests.

STAR METHODS

Detailed methods are provided in the online version of this paper and include the following:

- KEY RESOURCES TABLE
- EXPERIMENTAL MODEL AND STUDY PARTICIPANT DETAILS
 - Cells
 - Human CRC organoids
 - Mice
- METHOD DETAILS
 - CyDNA isolation
 - BMDC uptake of endogenous CRC DNA
 - BMDC CyDNA stimulations
 - BMDC and T cell Co-cultures
 - CyDNA Separation by FPLC
 - cGAS oligomerization
 - Electrophoretic mobility shift assay (EMSA)
 - MtDNA depletion and isolation
 - Microsatellite CyDNA pulldown
 - cGAS pulldown
 - Adoptive BMDC transfer
- QUANTIFICATION AND STATISTICAL ANALYSIS
 - scRNASeq
 - Sequencing

SUPPLEMENTAL INFORMATION

Supplemental information can be found online at <https://doi.org/10.1016/j.celrep.2024.115177>.

Received: April 12, 2024

Revised: November 10, 2024

Accepted: December 18, 2024

Published: January 24, 2025

REFERENCES

1. Xi, Y., and Xu, P. (2021). Global colorectal cancer burden in 2020 and projections to 2040. *Transl. Oncol.* 14, 101174. <https://doi.org/10.1016/j.tranon.2021.101174>.
2. Kuipers, E.J., Grady, W.M., Lieberman, D., Seufferlein, T., Sung, J.J., Boelens, P.G., van de Velde, C.J.H., and Watanabe, T. (2015). Colorectal cancer. *Nat. Publ. Gr.* 1, 15065. <https://doi.org/10.1038/nrdp.2015.65>.
3. Dekker, E., Tanis, P.J., Vleugels, J.L.A., Kasi, P.M., and Wallace, M.B. (2019). Colorectal cancer. *Lancet* 394, 1467–1480. [https://doi.org/10.1016/S0140-6736\(19\)32319-0](https://doi.org/10.1016/S0140-6736(19)32319-0).
4. Tennstedt, P., Fresow, R., Simon, R., Marx, A., Terracciano, L., Petersen, C., Sauter, G., Dikomey, E., and Borgmann, K. (2013). RAD51 overexpression is a negative prognostic marker for colorectal adenocarcinoma. *Int. J. Cancer* 132, 2118–2126. <https://doi.org/10.1002/ijc.27907>.
5. Kloos, M., and Von Knebel Doeberitz, M. (2016). The immune biology of microsatellite-unstable cancer. *Trends Cancer* 2, 121–133. <https://doi.org/10.1016/j.trecan.2016.02.004>.
6. Gelsomino, F., Barbolini, M., Spallanzani, A., Pugliese, G., and Cascinu, S. (2016). The evolving role of microsatellite instability in colorectal cancer: A review. *Cancer Treat Rev.* 51, 19–26. <https://doi.org/10.1016/j.ctrv.2016.10.005>.
7. Llosa, N.J., Cruise, M., Tam, A., Wicks, E.C., Hechenbleikner, E.M., Taube, J.M., Blosser, R.L., Fan, H., Wang, H., Luber, B.S., et al. (2015). The vigorous immune microenvironment of microsatellite instable colon cancer is balanced by multiple counter-inhibitory checkpoints. *Cancer Discov.* 5, 43–51. <https://doi.org/10.1158/2159-8290.CD-14-0863>.
8. Kim, S.R., Pina, A., Albert, A., Mcalpine, J.N., Wolber, R., Gilks, B., Carey, M.S., and Kwon, J.S. (2020). Mismatch repair deficiency and prognostic significance in patients with low-risk endometrioid endometrial cancers. *Int. J. Gynecol. Cancer* 30, 783–788. <https://doi.org/10.1136/ijgc-2019-00910>.
9. Mowat, C., Mosley, S.R., Namdar, A., Schiller, D., and Baker, K. (2021). Anti-tumor immunity in mismatch repair-deficient colorectal cancers requires type I IFN-driven CCL5 and CXCL10. *J. Exp. Med.* 218, e20210108. <https://doi.org/10.1084/jem.20210108>.
10. Schlee, M., and Hartmann, G. (2016). Discriminating self from non-self in nucleic acid sensing. *Nat. Rev. Immunol.* 16, 566–580. <https://doi.org/10.1038/nri.2016.78>.
11. Li, X., Shu, C., Yi, G., Chaton, C.T., Shelton, C.L., Diao, J., Zuo, X., Kao, C.C., Herr, A.B., and Li, P. (2013). Cyclic GMP-AMP Synthase Is Activated by Double-Stranded DNA-Induced Oligomerization. *Immunity* 39, 1019–1031. <https://doi.org/10.1016/j.immuni.2013.10.019>.
12. Ng, K.W., Marshall, E.A., Bell, J.C., and Lam, W.L. (2018). cGAS-STING and Cancer: Dichotomous Roles in Tumor Immunity and Development. *Trends Immunol.* 39, 44–54. <https://doi.org/10.1016/j.it.2017.07.013>.
13. Storozynsky, Q., and Hitt, M.M. (2020). The impact of radiation-induced dna damage on cgas-sting-mediated immune responses to cancer. *Int. J. Mol. Sci.* 21, 8877. <https://doi.org/10.3390/ijms21228877>.
14. Chabanon, R.M., Rouanne, M., Lord, C.J., Soria, J.C., Pasero, P., and Postel-Vinay, S. (2021). Targeting the DNA damage response in immuno-oncology: developments and opportunities. *Nat. Rev. Cancer* 21, 701–717. <https://doi.org/10.1038/s41568-021-00386-6>.
15. Zhu, Q., Man, S.M., Gurung, P., Liu, Z., Vogel, P., Lamkanfi, M., and Kangani, T.-D. (2014). Cutting Edge: STING Mediates Protection against Colorectal Tumorigenesis by Governing the Magnitude of Intestinal Inflammation. *J. Immunol.* 193, 4779–4782. <https://doi.org/10.4049/jimmunol.1402051>.
16. Deng, L., Liang, H., Xu, M., Yang, X., Burnette, B., Arina, A., Li, X.D., Maucceri, H., Beckett, M., Darga, T., et al. (2014). STING-dependent cytosolic DNA sensing promotes radiation-induced type I interferon-dependent antitumor immunity in immunogenic tumors. *Immunity* 41, 843–852. <https://doi.org/10.1016/j.immuni.2014.10.019>
17. Flood, B.A., Higgs, E.F., Li, S., Luke, J.J., and Gajewski, T.F. (2019). STING pathway agonism as a cancer therapeutic. *Immunol. Rev.* 290, 24–38. <https://doi.org/10.1111/imr.12765>.
18. Schadt, L., Sparano, C., Schweiger, N.A., Silina, K., Ceconni, V., Lucchiari, G., Yagita, H., Guggisberg, E., Saba, S., Nascaova, Z., et al. (2019). Cancer-Cell-Intrinsic cGAS Expression Mediates Tumor Immunogenicity. *Cell Rep.* 29, 1236–1248.e7. <https://doi.org/10.1016/j.celrep.2019.09.065>.
19. Vanpouille-Box, C., Demaria, S., Formenti, S.C., and Galluzzi, L. (2018). Cytosolic DNA Sensing in Organismal Tumor Control. *Cancer Cell* 34, 361–378. <https://doi.org/10.1016/j.ccr.2018.05.013>.
20. Rivera Vargas, T., Benoit-Lizon, I., and Apetoh, L. (2017). Rationale for stimulator of interferon genes-targeted cancer immunotherapy. *Eur. J. Cancer* 75, 86–97. <https://doi.org/10.1016/j.ejca.2016.12.028>.
21. Andreeva, L., Hiller, B., Kostrewa, D., Lässig, C., De Oliveira Mann, C.C., Jan Drexler, D., Maiser, A., Gaidt, M., Leonhardt, H., Hornung, V., and Hopfner, K.P. (2017). CGAS senses long and HMGB1/TFAM-bound U-turn DNA by forming protein-DNA ladders. *Nature* 549, 394–398. <https://doi.org/10.1038/nature23890>.

22. Wiser, C., Kim, B., Vincent, J., and Ascano, M. (2020). Small molecule inhibition of human cGAS reduces total cGAMP output and cytokine expression in cells. *Sci. Rep.* 10, 7604. <https://doi.org/10.1038/s41598-020-64348-y>.
23. Longley, D.B., Harkin, D.P., and Johnston, P.G. (2003). 5-fluorouracil: mechanisms of action and clinical strategies. *Nat. Rev. Cancer* 3, 330–338. <https://doi.org/10.1038/nrc1074>.
24. West, A.P., Khouri-Hanold, W., Staron, M., Tal, M.C., Pineda, C.M., Lang, S.M., Bestwick, M., Duguay, B.A., Raimundo, N., MacDuff, D.A., et al. (2015). Mitochondrial DNA stress primes the antiviral innate immune response. *Nature* 520, 553–557. <https://doi.org/10.1038/nature14156>.
25. Yu, C.H., Davidson, S., Harapas, C.R., Hilton, J.B., Mlodzianoski, M.J., Laohamonthonkul, P., Louis, C., Low, R.R.J., Moecking, J., De Nardo, D., et al. (2020). TDP-43 Triggers Mitochondrial DNA Release via mPTP to Activate cGAS/STING in ALS. *Cell* 183, 636–649.e18. <https://doi.org/10.1016/j.cell.2020.09.020>.
26. De Cecco, M., Ito, T., Petraschen, A.P., Elias, A.E., Skvir, N.J., Criscione, S.W., Caligiana, A., Brocculi, G., Adney, E.M., Boeke, J.D., et al. (2019). L1 drives IFN in senescent cells and promotes age-associated inflammation. *Nature* 566, 73–78. <https://doi.org/10.1038/s41586-018-0784-9>.
27. Lindholm, H.T., Chen, R., and De Carvalho, D.D. (2023). Endogenous retroelements as alarms for disruptions to cellular homeostasis. *Trends Cancer* 9, 55–68. <https://doi.org/10.1016/j.trecan.2022.09.001>.
28. Smit, A., Hubley, R., and Green, P. RepeatMasker Open-4.0. <http://www.repeatmasker.org>.
29. Lo, J., Jonika, M.M., and Blackmon, H. (2019). micRoCounter: Microsatellite characterization in genome assemblies. *G3 (Bethesda)* 9, 3101–3104. <https://doi.org/10.1534/g3.119.400335>.
30. Bourque, G., Burns, K.H., Gehring, M., Gorbunova, V., Seluanov, A., Hammell, M., Imbeault, M., Izsák, Z., Levin, H.L., Macfarlan, T.S., et al. (2018). Ten things you should know about transposable elements. *Genome Biol.* 19, 1–12. <https://doi.org/10.1186/s13059-018-1577-z>.
31. Arensburger, P., Hice, R.H., Zhou, L., Smith, R.C., Tom, A.C., Wright, J.A., Knapp, J., O'Brochta, D.A., Craig, N.L., and Atkinson, P.W. (2011). Phylogenetic and functional characterization of the hAT transposon superfamily. *Genetics* 188, 45–57. <https://doi.org/10.1534/genetics.111.126813>.
32. Riley, J.S., and Tait, S.W. (2020). Mitochondrial DNA in inflammation and immunity. *EMBO Rep.* 21, e49799. <https://doi.org/10.15252/embr.201949799>.
33. Warren, E.B., Aicher, A.E., Fessel, J.P., and Konradi, C. (2017). Mitochondrial DNA depletion by ethidium bromide decreases neuronal mitochondrial creatine kinase: Implications for striatal energy metabolism. *PLoS One* 12, e0190456. <https://doi.org/10.1371/journal.pone.0190456>.
34. Xian, H., Watari, K., Sanchez-Lopez, E., Offenberger, J., Onyuru, J., Sampath, H., Ying, W., Hoffman, H.M., Shadel, G.S., and Karin, M. (2022). Oxidized DNA fragments exit mitochondria via mPTP- and VDAC-dependent channels to activate NLRP3 inflammasome and interferon signaling. *Immunity* 55, 1370–1385.e8. <https://doi.org/10.1016/j.jimmuni.2022.06.007>.
35. Hao, Z., Wu, T., Cui, X., Zhu, P., Tan, C., Dou, X., Hsu, K.W., Lin, Y.T., Peng, P.H., Zhang, L.S., et al. (2020). N6-Deoxyadenosine Methylation in Mammalian Mitochondrial DNA. *Mol. Cell* 78, 382–395.e8. <https://doi.org/10.1016/j.molcel.2020.02.018>.
36. Zhong, F., Liang, S., and Zhong, Z. (2019). Emerging Role of Mitochondrial DNA as a Major Driver of Inflammation and Disease Progression. *Trends Immunol.* 40, 1120–1133. <https://doi.org/10.1016/j.it.2019.10.008>.
37. Jiao, Y., Nan, J., Mu, B., Zhang, Y., Zhou, N., Yang, S., Zhang, S., Lin, W., Wang, F., Xia, A., et al. (2022). Discovery of a novel and potent inhibitor with differential species-specific effects against NLRP3 and AIM2 inflammasome-dependent pyroptosis. *Eur. J. Med. Chem.* 232, 114194. <https://doi.org/10.1016/j.ejmech.2022.114194>.
38. Le, D.T., Uram, J.N., Wang, H., Bartlett, B.R., Kemberling, H., Eyring, A.D., Skora, A.D., Luber, B.S., Azad, N.S., Laheru, D., et al. (2015). PD-1 Blockade in Tumors with Mismatch-Repair Deficiency. *N. Engl. J. Med.* 372, 2509–2520. <https://doi.org/10.1056/nejmoa1500596>.
39. Wculek, S.K., Cueto, F.J., Mujal, A.M., Melero, I., Krummel, M.F., and Sanchez, D. (2020). Dendritic cells in cancer immunology and immunotherapy. *Nat. Rev. Immunol.* 20, 7–24. <https://doi.org/10.1038/s41577-019-0210-z>.
40. Guan, J., Lu, C., Jin, Q., Lu, H., Chen, X., Tian, L., Zhang, Y., Ortega, J., Zhang, J., Siteni, S., et al. (2021). MLH1 Deficiency-Triggered DNA Hyperexcision by Exonuclease 1 Activates the cGAS-STING Pathway. *Cancer Cell* 39, 109–121.e5. <https://doi.org/10.1016/j.ccr.2020.11.004>.
41. Wang, J., Li, S., Wang, M., Wang, X., Chen, S., Sun, Z., Ren, X., Huang, G., Sumer, B.D., Yan, N., et al. (2024). STING licensing of type I dendritic cells potentiates antitumor immunity. *Sci. Immunol.* 9, eadj3945. <https://doi.org/10.1126/sciimmunol.adj3945>.
42. Xie, W., Lama, L., Adura, C., Tomita, D., Glickman, J.F., Tuschi, T., and Patel, D.J. (2019). Human cGAS catalytic domain has an additional DNA-binding interface that enhances enzymatic activity and liquid-phase condensation. *Proc. Natl. Acad. Sci. USA* 116, 11946–11955. <https://doi.org/10.1073/pnas.1905013116>.
43. Herzner, A.M., Hagmann, C.A., Goldeck, M., Wolter, S., Kübler, K., Wittmann, S., Gramberg, T., Andreeva, L., Hopfner, K.P., Mertens, C., et al. (2015). Sequence-specific activation of the DNA sensor cGAS by Y-form DNA structures as found in primary HIV-1 cDNA. *Nat. Immunol.* 16, 1025–1033. <https://doi.org/10.1038/ni.3267>.
44. Gentili, M., Lahaye, X., Nadalin, F., Nader, G.P.F., Puig Lombardi, E., Hervé, S., De Silva, N.S., Rookhuizen, D.C., Zueva, E., Goudot, C., et al. (2019). The N-Terminal Domain of cGAS Determines Preferential Association with Centromeric DNA and Innate Immune Activation in the Nucleus. *Cell Rep.* 26, 2377–2393.e13. <https://doi.org/10.1016/j.celrep.2019.01.105>.
45. Zhao, X., Li, L., Starr, T.K., and Subramanian, S. (2017). Tumor location impacts immune response in mouse models of colon cancer. *Oncotarget* 8, 54775–54787. <https://doi.org/10.18632/oncotarget.18423>.
46. Killion, J.J., Radinsky, R., and Fidler, I.J. (1998). Orthotopic models are necessary to predict therapy of transplantable tumors in mice. *Cancer Metastasis Rev.* 17, 279–284. <https://doi.org/10.1023/A:1006140513233>.
47. Fung, A.S., Lee, C., Yu, M., and Tannock, I.F. (2015). The effect of chemotherapeutic agents on tumor vasculature in subcutaneous and orthotopic human tumor xenografts. *BMC Cancer* 15, 112. <https://doi.org/10.1186/s12885-015-1091-6>.
48. Balzarolo, M., Engels, S., De Jong, A.J., Franke, K., Van Den Berg, T.K., Gulen, M.F., Ablässer, A., Janssen, E.M., Van Steensel, B., and Wolkers, M.C. (2021). M6A methylation potentiates cytosolic dsDNA recognition in a sequence-specific manner. *Open Biol.* 11, 210030. <https://doi.org/10.1098/rsob.210030>.
49. MacDonald, K.M., Nicholson-Puthenveedu, S., Tageldein, M.M., Khasnis, S., Arrowsmith, C.H., and Harding, S.M. (2023). Antecedent chromatin organization determines cGAS recruitment to ruptured micronuclei. *Nat. Commun.* 14, 556. <https://doi.org/10.1038/s41467-023-36195-8>.
50. Baker, K., Qiao, S.W., Kuo, T.T., Aveson, V.G., Platzer, B., Andersen, J.T., Sandlie, I., Chen, Z., De Haar, C., Lencer, W.I., et al. (2011). Neonatal Fc receptor for IgG (FcRn) regulates cross-presentation of IgG immune complexes by CD8-CD11b+ dendritic cells. *Proc. Natl. Acad. Sci. USA* 108, 9927–9932. <https://doi.org/10.1073/pnas.1019037108>.
51. Sato, T., Stange, D.E., Ferrante, M., Vries, R.G.J., Van Es, J.H., Van Den Brink, S., Van Houdt, W.J., Pronk, A., Van Gorp, J., Siersma, P.D., and Clevers, H. (2011). Long-term expansion of epithelial organoids from human colon, adenoma, adenocarcinoma, and Barrett's epithelium. *Gastroenterology* 141, 1762–1772. <https://doi.org/10.1053/j.gastro.2011.07.050>.
52. Miyoshi, H., and Stappenbeck, T.S. (2013). In vitro expansion and genetic modification of gastrointestinal stem cells in spheroid culture. *Nat. Protoc.* 8, 2471–2482. <https://doi.org/10.1038/nprot.2013.153>.
53. Moffat, J., Grueneberg, D.A., Yang, X., Kim, S.Y., Kloepfer, A.M., Hinkle, G., Piqani, B., Eisenhaure, T.M., Luo, B., Grenier, J.K., et al. (2006). A

- Lentiviral RNAi Library for Human and Mouse Genes Applied to an Arrayed Viral High-Content Screen. *Cell* 124, 1283–1298. <https://doi.org/10.1016/j.cell.2006.01.040>.
54. Koo, B.K., Stange, D.E., Sato, T., Karthaus, W., Farin, H.F., Huch, M., Van Es, J.H., and Clevers, H. (2011). Controlled gene expression in primary Lgr5 organoid cultures. *Nat. Methods* 9, 81–83. <https://doi.org/10.1038/nmeth.1802>.
 55. Roper, J., Tammela, T., Akkad, A., Almeqdadi, M., Santos, S.B., Jacks, T., and Yilmaz, Ö.H. (2018). Colonoscopy-based colorectal cancer modeling in mice with CRISPR-Cas9 genome editing and organoid transplantation. *Nat. Protoc.* 13, 217–234. <https://doi.org/10.1038/nprot.2017.136>.
 56. Mosley, S.R., and Baker, K. (2022). Isolation of endogenous cytosolic DNA from cultured cells. *STAR Protoc.* 3, 101165. <https://doi.org/10.1016/j.xpro.2022.101165>.
 57. St. John, J., and Quinn, T.W. (2008). Rapid capture of DNA targets. *Bio-techniques* 44, 259–264. <https://doi.org/10.2144/000112633>.
 58. Subramanian, A., Tamayo, P., Mootha, V.K., Mukherjee, S., Ebert, B.L., Gillette, M.A., Paulovich, A., Pomeroy, S.L., Golub, T.R., Lander, E.S., and Mesirov, J.P. (2005). Gene set enrichment analysis: A knowledge-based approach for interpreting genome-wide expression profiles. *Proc. Natl. Acad. Sci. USA* 102, 15545–15550. <https://doi.org/10.1073/pnas.0506580102>.
 59. Cock, P.J.A., Antao, T., Chang, J.T., Chapman, B.A., Cox, C.J., Dalke, A., Friedberg, I., Hamelryck, T., Kauff, F., Wilczynski, B., and de Hoon, M.J.L. (2009). Biopython: Freely available Python tools for computational molecular biology and bioinformatics. *Bioinformatics* 25, 1422–1423. <https://doi.org/10.1093/bioinformatics/btp163>.
 60. Andrews, S. (2010). Fast QC: A quality control tool for high throughput sequence data [online]. Available online at: <http://www.bioinformatics.babraham.ac.uk/projects/fastqc/>.
 61. Morgan, M., Pages, H., Obenchain, V., and Hayden, N. (2021). Rsamtools: Binary alignment (BAM), FASTA, variant call (BCF), and tabix file import. R package version 2.10.0. <https://bioconductor.org/packages/Rsamtools>.
 62. Lawrence, M., Gentleman, R., and Carey, V. (2009). rtracklayer: An R package for interfacing with genome browsers. *Bioinformatics* 25, 1841–1842. <https://doi.org/10.1093/bioinformatics/btp328>.
 63. Lawrence, M., Huber, W., Pagès, H., Aboyoun, P., Carlson, M., Gentleman, R., Morgan, M.T., and Carey, V.J. (2013). Software for Computing and Annotating Genomic Ranges. *PLoS Comput. Biol.* 9, 1–10. <https://doi.org/10.1371/journal.pcbi.1003118>.
 64. Yue, F., Cheng, Y., Breschi, A., Vierstra, J., Wu, W., Ryba, T., Sandstrom, R., Ma, Z., Davis, C., Pope, B.D., et al. (2014). A comparative encyclopedia of DNA elements in the mouse genome. *Nature* 515, 355–364. <https://doi.org/10.1038/nature13992>.
 65. Bushnell, B., Rood, J., and Singer, E. (2017). BBMerge – Accurate paired shotgun read merging via overlap. *PLoS One* 12, e0185056. <https://doi.org/10.1371/journal.pone.0185056>.

STAR★METHODS

KEY RESOURCES TABLE

| REAGENT or RESOURCE | SOURCE | IDENTIFIER |
|-------------------------------------------------------------------------------------|---------------------------|------------------------------|
| Antibodies | | |
| IFNg-PE | Thermo Fisher Scientific | 12-7311-82; RRID:AB_466193 |
| CD69-Alexa ⁷⁰⁰ | Thermo Fisher Scientific | 56-0691-82; RRID:AB_2815240 |
| Ki67-PECy5 | Thermo Fisher Scientific | 15-5698-82; RRID:AB_2802209 |
| pTBK1 | Cell Signaling Technology | 5483S; RRID:AB_10693472 |
| TBK1 | Cell Signaling Technology | 3504S; RRID:AB_2255663 |
| pSTAT1 | Thermo Fisher Scientific | 33-3400; RRID:AB_2533113 |
| STAT1 | Cell Signaling Technology | 9172L; RRID:AB_2198300 |
| GAPDH | Thermo Fisher Scientific | MA5-15738; RRID:AB_10977387 |
| pSTING | Cell Signaling Technology | 72971S; RRID:AB_2799831 |
| βActin | Cell Signaling Technology | 8457L; RRID:AB_10950489 |
| pNF-κB | Cell Signaling Technology | 3033S; RRID:AB_331284 |
| cGAS | Cell Signaling Technology | 31659S; RRID:AB_2799008 |
| Anti-Rabbit IgG Isotype Control | Thermo Fisher Scientific | 02-6102; RRID:AB_2532938 |
| MHCII-PECy5 | Thermo Fisher Scientific | 15-5321-82; RRID:AB_468800 |
| CD8-Alexa ⁷⁰⁰ | Thermo Fisher Scientific | 56-0081-82; RRID:AB_494005 |
| CD45-PE | Thermo Fisher Scientific | 12-0451-83; RRID:AB_465669 |
| CD86-APCCy7 | Thermo Fisher Scientific | 47-0862-82; RRID:AB_2815162 |
| CD103-PE | Thermo Fisher Scientific | 12-1031-83; RRID:AB_465800 |
| CD11c-Alexa ⁷⁰⁰ | BD Biosciences | 560583; RRID:AB_1727421 |
| CD11b-PECy7 | Thermo Fisher Scientific | 25-0112-82; RRID:AB_469588 |
| PD-L1-Alexa ⁷⁵⁰ | Thermo Fisher Scientific | 47-5983-42; RRID:AB_2688259 |
| Peroxidase-AffiniPure Goat Anti-Rabbit IgG (H+L) (min X Hu,Ms,Rat Sr Prot) | Jackson Immunoresearch | 111-035-144; RRID:AB_2307391 |
| Peroxidase-AffiniPure Goat Anti-Mouse IgG (H+L) (min X Hu,Bov,Hrs,Rb,Sw Sr Prot) | Jackson Immunoresearch | 115-035-146; RRID:AB_2307392 |
| Alexa Fluor 594-AffiniPure Goat Anti-Rabbit IgG (H+L) (min X Hu Sr Prot) | Jackson Immunoresearch | 111-585-045; RRID:AB_2338062 |
| Bacterial and virus strains | | |
| pLKO.1 | Addgene | 24150; RRID:Addgene_24150 |
| Biological samples | | |
| L-cells expressing Wnt3a, R-Spondin and Noggin | ATCC | CRL-3276; RRID:CVCL_DA06 |
| Chemicals, peptides, and recombinant proteins | | |
| Oxaliplatin | Thermo Fisher Scientific | AC456131000 |
| Digitonin | Millipore Sigma | 11024-24-1 |
| Hexylene Glycol | Fisher Scientific | AAL03187AP |
| Proteinase K | Fisher Scientific | BP1700-500 |
| RNase A | Thermo Fisher Scientific | EN0531 |
| Phenol-chloroform isoamyl alcohol | Fisher Scientific | BP1752I-400 |
| Lipofectamine 2000 | Thermo Fisher Scientific | 11668019 |
| Herring Sperm DNA (HT-DNA) | Thermo Fisher Scientific | 15634-017 |
| Trizol | Thermo Fisher Scientific | 15596026 |
| OVA protein | Millipore Sigma | A5378 |
| Collagenase XI | Millipore Sigma | C5138 |
| Dispase II | Millipore Sigma | D4693 |
| Matrigel Growth Factor Reduced (GFR) | Corning | 354230 |

(Continued on next page)

Continued

| REAGENT or RESOURCE | SOURCE | IDENTIFIER |
|-------------------------------------------------------|------------------------------|---------------------------|
| N-Acetylcysteine | Thermo Fisher Scientific | 160280250 |
| N2 supplement | Thermo Fisher Scientific | 17502048 |
| B27 supplement | Thermo Fisher Scientific | 17504044 |
| Nicotinamide | Millipore Sigma | N0636 |
| A83-01 | Millipore Sigma | SML0788 |
| SB202190 | Millipore Sigma | S7067 |
| EGF | Thermo Fisher Scientific | PMG8043 |
| TrypLE Express | Thermo Fisher Scientific | 12605028 |
| Polybrene | Sigma-Aldrich | H9268 |
| Y27632 | Sigma-Aldrich | Y0503 |
| Hygromycin | Thermo Fisher Scientific | 10687010 |
| Cell Recovery Solution | Corning | 354253 |
| NEB Buffer 2 | NEB | B7002S |
| PicoGreen | Thermo Fisher Scientific | P7581 |
| RU-521 cGAS Inhibitor | Cayman Chemicals | 31765 |
| IN-3 AIM2 and NLRP3 Inhibitor | Med Chem Express | HY-144226 |
| PMA | Millipore Sigma | P1585 |
| Ionomycin | Thermo Fisher Scientific | J60628 |
| Monensin | Thermo Fisher Scientific | 00-4505-51 |
| SYBR Gold | Thermo Fisher Scientific | S11494 |
| Ethidium Bromide (EtBr) | Fisher Scientific | BP1302-10 |
| Recombinant human cGAS protein | Cayman Chemicals | 22810 |
| EasySep Streptavidin magnetic beads | StemCell | 50001 |
| rCutSmart Buffer | NEB | B6004S |
| EcoRV-HF | NEB | R3195L |
| DNasel | Thermo Fisher Scientific | D2821 |
| Critical commercial assays | | |
| Bioanalyzer High Sensitivity DNA Kit | Agilent | 5067-4626 |
| Click-iT EdU Cell Proliferation Kit | Thermo Fisher Scientific | C10419 |
| High-Capacity cDNA Reverse Transcriptase Kit | Applied Biosystems | 4368814 |
| PowerUp SYBR Green Master Mix | Applied Biosystems | A25742 |
| EasySep Mouse CD8 ⁺ T cell Isolation Kit | StemCell | 19853A |
| Zombie Aqua Fixable Viability Kit | BioLegend | 423102 |
| FOXP3/Transcription Factor Staining Kit | eBioscience | 00-5523-00 |
| Pierce BCA Protein Assay Kit | Thermo Fisher Scientific | 23225 |
| Mini-Y Adapter Library kit | Lucigen | N/A |
| Qubit ssDNA Assay Kit | Thermo Fisher Scientific | Q10212 |
| Mitochondrial DNA Isolation Kit | Abcam | AB65321 |
| Qiaprep Spin Miniprep Kit | Qiagen | 27106 |
| GeneJet Genomic DNA Purification Kit | Thermo Fisher Scientific | K0722 |
| NEB Quick Blunting Kit | NEB | E1201L |
| T4 DNA Ligase Kit | NEB | M0202L |
| Q5 High-Fidelity DNA Polymerase Kit | NEB | M0491L |
| CFDA | Thermo Fisher Scientific | V12883 |
| Deposited data | | |
| scRNASeq of orthotopic MSI and CIN tumors | NCBI Gene Expression Omnibus | GSE178706 |
| cyDNA sequencing of MC38 MSI and CIN CRC | NCBI Sequence Read Archive | PRJNA1152723 |
| Experimental models: Cell lines | | |
| MC38 Cells (C57BL/6 Mouse, Colorectal Cancer, Female) | Kerafast | ENH204-FP; RRID:CVCL_B288 |

(Continued on next page)

Continued

| REAGENT or RESOURCE | SOURCE | IDENTIFIER |
|---------------------------------------------------------------------------|---------------|------------------------------|
| Experimental models: Organisms/strains | | |
| C57BL/6 Mice (C57BL/6NCrl) | Charles River | 027; RRID:IMSR_CRL:027 |
| C57BL/6 OT-1 Mice (C57BL/6-Tg(TcrαTcrβ)1100Mjb/J) | JAX | 003831; RRID:IMSR_JAX:003831 |
| <i>Sting</i> ^{Gt} Mice (C57BL/6J- <i>Sting</i> ^{Gt} /J) | JAX | 017537; RRID:IMSR_JAX:017537 |
| Oligonucleotides | | |
| 30bp Oligo 1 Fwd: TCTTTAGAGGCCCGCGTTACGACTTCAT | IDT | N/A |
| 30bp Oligo 1 Rev: ATGAAGTCGAAACGCGGGCTCTGAAAGA | IDT | N/A |
| 30bp Oligo 2 Fwd: AATATACCGTGTTCAGCCGGTAGCTTATT | IDT | N/A |
| 30bp Oligo 2 Rev: AATAAGCTACCCGGCTGAACACGGTATATT | IDT | N/A |
| 30bp Oligo 3 Fwd: GCGGCTGTGATGTTGCCATCGAGAAAGAT | IDT | N/A |
| 30bp Oligo 3 Rev: ATCTTCTCGATGGCAAAACATCACAGCCGC | IDT | N/A |
| 50bp Oligo 1 Fwd: CCTCACGTCGAGTTCACTGTCGGCATAT | IDT | N/A |
| GCTATCCGTAGCAAAATTCCC | | |
| 50bp Oligo 1 Rev: GGGAAATTTCGACGGATAAGCATATGCCG | IDT | N/A |
| ACACTGAAACTCGACGTGAGG | | |
| 50bp Oligo 2 Fwd: GTCATGAATCAATCGCACTGAGTGAATTG | IDT | N/A |
| TGAAAGAAATGAGGTAGCTT | | |
| 50bp Oligo 2 Rev: AAGCTACCTCATTCTTCACGAATTCACTC | IDT | N/A |
| AGTGCATTGATTGATGAC | | |
| 50bp Oligo 3 Fwd: GCGATCGTCTTATCTGCACCGTGCAAAC | IDT | N/A |
| CCAAGCTACCATTGCGTGA | | |
| 50bp Oligo 3 Rev: TACACGCAATGGTAGCTTGAGTTGCACG | IDT | N/A |
| CGTGCAGATAAGACGATCGC | | |
| 70bp Oligo 1 Fwd: CTCCGGCGCCAAGAGTATTGGGTCTAT | IDT | N/A |
| CCACTGGTCAGCAAATGTGCCATATGAAGCAAGTAACACG | | |
| 70bp Oligo 1 Rev: CGTGTACTTGCTCATATGGCACAGTTG | IDT | N/A |
| CTGACCAGTGGATAGGACCAATACTCTTGGCGCCGGAG | | |
| 70bp Oligo 2 Fwd: GGCAAGCAGGCCCTCTCATCGTATATCA | IDT | N/A |
| ACGTGTCGTTGAGATATCAGTGTCTCTTCCGGTAA | | |
| 70bp Oligo 2 Rev: TTAAACGGGAAAGAGAACACTGATATCTCA | IDT | N/A |
| AACGGACACGTTGATACGCATGAGAAGGCCTGCTTGC | | |
| 70bp Oligo 3 Fwd: GGCACTCAGATGCATCGAACATCGGCCGA | IDT | N/A |
| TAGCTCCGGTAAGAAGTAAGACATGTACCCAAAGTTGAGT | | |
| 70bp Oligo 3 Rev: ACTACAACTTGGGTACATGTCTTACTCTTA | IDT | N/A |
| CCGGGAGCTATCCGGCATGTTGATGCATCTGAGTGCC | | |
| 200bp Oligo (Scramble 1) Fwd: TTAATAACATCGAGCATTAGGG | IDT | N/A |
| AGCCGCTAGTTGATTTGATTAATAACAAGGACTGTCCCTATT | | |
| AACCTTGGCGATCTGAAGCGACACCGTGTACTTGATGCCA | | |
| CAAGAGTAACCGAACCTAATTATGCCGTCGGGAGCGTTGC | | |
| CTGTCGTCTCTAGCCAATGTATACCATCAAGGTGAACCGCTT | | |
| AGTTAGGA | | |
| 200bp Oligo (Scramble 1) Rev: TCCTAACTAACGGTTCACCTT | IDT | N/A |
| GATGGTATACTTGGCTAGAACGACAGGCAACGCTCCCG | | |
| ACGGCGATAATTAAAGTTGCTACTTGTGATCAAGTAA | | |
| CACGGTGTGCTTCAGATCCGGCAAGGTTAATAGGGACAGT | | |
| CCTTGTATTAAATACAATCGAACATAGCGGCTCCCTAATGCTC | | |
| GATGTTATTAA | | |
| Scramble 2 Oligo Fwd: ATGTCCTGGCACCCCTGAAAAATGCT | IDT | N/A |
| GATGAGGTAATGGTACTAGCTTCCATTTCGCGGTCGA | | |
| GGGTTGGCATGAAAATCCAGTGATTGACATAGCACGCAC | | |
| ACACTGTCCTACATGGTTCGACAAGTGTGACCGAGACAT | | |
| ACAGCGTCAAACGGGAATCAACTAAGGACTAGAGGCC | | |
| ACTACCTATAGAGATG | | |

(Continued on next page)

Continued

| REAGENT or RESOURCE | SOURCE | IDENTIFIER |
|-------------------------------------------------------------------------------------------------------------------------------------------------------------------------------------------------------------------------------------------------------------|--------|------------|
| Scramble 2 Oligo Rev: CATCTCTATAGGTAGTGGGCCTCT AGTCCTTAGTTGATCCCGTTTGACGCTGTGCTGGTC ACACTTGTGCGAACCATGTTAGGGACAGTGTGCGTGC TATGTCAATCACTGGATTTCATGCCAACCTCGACC GCGAAAATAGGAAGCTAGTAGACCATTACCTCATCAG CATTTCAGGGTGCCAGGACAT | IDT | N/A |
| Microsatellite Edge Oligo 1 Fwd: AGTTGCAGACGTTGGCT CAGGTCAGGCTTATTGTAGCAAAGTCTACAAAGCAGTT CTAAGTGACCTTATTGTGACTGGCTCTAAAGGAAGGCG AGAGCCTGGTCTACAAAGTGAAGCTCCAAGACAGGCCAGG GCTACACAGAGAAACCTGTCTGGAAAAAAACAAAAAAACA AAAAACAACAACAACAACAAAAAAG | IDT | N/A |
| Microsatellite Edge Oligo 1 Rev: CTTTTTGTGTTGTTGTT GTTGTTTTGTTTTGTTTTTCAGACAGGGTTCTG TGTAGCCCCTGGCTGTCTGGAGCTCACTTGAGACAG GCTCTCGCCTCCTTAGAGCCAGTCACAATAAGGTC CTTAGAACTGCTTGTAGACTTTGCTACAATAAGCCTGGA CCTGAGCCAACGCTGCAACT | IDT | N/A |
| Microsatellite Edge Oligo 2 Fwd: AACACAACAACAACAA CAACAACAAAAAAAAAAACTGCTTACCCCTATGTAG TAACCTCTGCACCACTGGAGGACAGAGGAAGATGTAGG GTGTGCTGTTCTAAATTCCCACCTCCTTCAACCAT ATCTTACCAACAGAGAACATGGGGAAATGGGCAGACA TAGCTGTTCTAAATGAATATTAGGCA | IDT | N/A |
| Microsatellite Edge Oligo 2 Rev: TGCCATAATTCTATTAG AAAGACAGCTATGCTGCCATTTCCTCATGTTCTG TTGGTAAGATATGGTGAAGAAGGAGAGTGGGAATATTAG AACAGCACACCCCTACATCTCCTCTGTCCTCACTGGTG CAGAAGTTACTACATAGGGTAAGCAGAGTTTTTTTT GTTGTTGTTGTTGTTGTTGTT | IDT | N/A |
| Microsatellite Middle Oligo 1 Fwd: TAAGCATAAAACAA TTCCCTTACCAAGGAGGCAATCATGCATATGGTACAAGGA GGAAACTAACAAAAACAAAAGACCAAAAAACCCAAAAAA CAACAACAACAACACAAAACCTGTGCCTTATCCAATG CTATCCACCTTCATCCACTAAGTCATAATAGAATGCAA ATGGTAAGCTAGATGCCTCATGATTGCT | IDT | N/A |
| Microsatellite Middle Oligo 1 Rev: AGCAATCATGAGGCAT CTAGCTTACCATTCGATTCTATTATGCAGTTAGTGGATG AAGGTGGATAGCATTGGATAAGGCACAGGTTTTGTTG TGTGTTGTTGTTGGTTGGTTGGTCTTTGTTGTTGTTG TAGTTCCCTCCTGTACCATATGCATGATTGCCTCCTGGT AAGGAAATTGGTTTGATGCTTA | IDT | N/A |
| Microsatellite Middle Oligo 2 Fwd: TTGGTTATCATCACCA GGGCCCCGGGAGAACATTTCCTTACTTCCTTTCATTCT TCTATCCTAGTCTGGTTCAGTTGCTGTGATTAAACAA AACAAAACAACAACAACAACAAAACAAAAACAC TTGGGGAGAAAGTGTCTTAGGCTCACACATCCTGA TCATAGTCCATCAAGGAGGGAGTCAGGGC | IDT | N/A |
| Microsatellite Middle Oligo 2 Rev: GCCCTGACTTCCCTCCTT GATGGACTATGATCAGGATGTGTGAGCCTAAGAAACACTT TCTTCCCCAAGTTGTTTGTGTTGTTGTTGTTGTTGTTG TTGTTTGTGTTAAATCACAGCAACTGAACCAGACTAGGA TAGAAGGAAATGAAAGGAAGTAAAAATGTTCTCCCGGG CCCTGGTGTGATAACCAA | IDT | N/A |
| 10bp Scramble Probe (S2): Biotin-TACAGCGACG | IDT | N/A |
| 15bp Scramble Probe (S3): Biotin-CAGCATTAGCGTAGA | IDT | N/A |

(Continued on next page)

Continued

| REAGENT or RESOURCE | SOURCE | IDENTIFIER |
|-----------------------------------------------------------------|--------------------------|----------------|
| CA ₅ Probe: Biotin-CACACACACA | IDT | N/A |
| TC ₅ Probe: Biotin-TCTCTCTCTC | IDT | N/A |
| TG ₅ Probe: Biotin-TGTGTGTGTG | IDT | N/A |
| TGG ₅ Probe: Biotin-TGGTGGTGGTGGTGG | IDT | N/A |
| GTT ₅ Probe: Biotin-GTTGTTGTTGTTGTT | IDT | N/A |
| GGAA ₅ Probe: Biotin-GGAAGGAAGGAAGGAAGGAA | IDT | N/A |
| Pulldown Adapter 1 Fwd: GTCTCCTCTGACTTCAACAGCGGATATC | IDT | N/A |
| Pulldown Adapter 1 Rev: GATATCCGCTGTTGAAGTCAGAGGAGACC | IDT | N/A |
| Pulldown Adapter 2 Fwd: GATATCACCCACCTGTTGCTGTAGCCAA | IDT | N/A |
| Pulldown Adapter 2 Rev: TTTGGCTACAGCAACAGGGTGGTGTATTC | IDT | N/A |
| GAPDH qPCR Primer Fwd: CATTTCCAGTATGACTCCA | IDT | N/A |
| GAPDH qPCR Primer Rev: TGAAGACACCAGTAGACTCC | IDT | N/A |
| IFN β qPCR Primer Fwd: CGTGGGAGATGCCTCAACT | IDT | N/A |
| IFN β qPCR Primer Rev: AGATCTCTGCTCGGACCACC | IDT | N/A |
| CXCL10 qPCR Primer Fwd: CCAAGTGCTGCCGTATTTC | IDT | N/A |
| CXCL10 qPCR Primer Rev: GGCTCGCAGGGATGATTCAA | IDT | N/A |
| CCL5 qPCR Primer Fwd: GCTGCTTGCCCTACCTCTCC | IDT | N/A |
| CCL5 qPCR Primer Rev: TCGAGTGACAAACACGACTGC | IDT | N/A |
| IRF7 qPCR Primer Fwd: GGTGTGCCCCAGGATCATT | IDT | N/A |
| IRF7 qPCR Primer Rev: GCTGCATAGGGTCCCTCGTAA | IDT | N/A |
| IFN α qPCR Primer Fwd: GGATGTGACCTTCCTCAGACTC | IDT | N/A |
| IFN α qPCR Primer Rev: ACCTTCTCCTGCGGGAAATCCAA | IDT | N/A |
| mtDNA 1 qPCR Primer Fwd: AACGGATCCACAGCCGTA | IDT | N/A |
| mtDNA 1 qPCR Primer Rev: AGTCCTCGGGCCATGATT | IDT | N/A |
| mtDNA 2 qPCR Primer Fwd: CAAACACTTATTACAACCCAAGAACAA | IDT | N/A |
| mtDNA 2 qPCR Primer Rev: TCATATTATGGCTATGGTCAGG | IDT | N/A |
| Pulldown Adapter PCR Primer Fwd: GTCTCCTCTGACTTCAACAGCG | IDT | N/A |
| Pulldown Adapter PCR Primer Rev: ACCACCCTGTTGCTGTAGCCAA | IDT | N/A |
| Scramble 2 Oligo qPCR Primer Fwd: CACACTGTCCTACATGGTC | IDT | N/A |
| Scramble 2 Oligo qPCR Primer Rev: TTTGACGCTGTATGTCGGTC | IDT | N/A |
| Microsatellite Edge 2 qPCR Primer Fwd: GATGTAGGGTGTGCTGTTCTAA | IDT | N/A |
| Microsatellite Edge 2 qPCR Primer Rev: CCCATGTTCTCTGTTGGTAAGA | IDT | N/A |
| Microsatellite Middle 2 qPCR Primer Fwd: GAAAGTGTCTCTAGGCTCACAC | IDT | N/A |
| Microsatellite Middle 2 qPCR Primer Rev: CTCCCTCCTGATGGACTATG | IDT | N/A |
| Software and algorithms | | |
| FlowJo | FlowJo | N/A |
| GraphPad Prism 8 | GraphPad | N/A |
| Inkscape | Inkscape | N/A |
| BioRender | BioRender.com | N/A |
| Other | | |
| Nanodrop 1000 | Thermo Fisher Scientific | ND-1000 UV/Vis |
| QuantStudio 6 Real-Time PCR System | Applied Biosystems | N/A |
| CytoFlex S Flow Cytometer | Beckman Coulter | N/A |
| Bioanalyzer 2100 | Agilent | N/A |
| Akta Explorer 10 | Cytiva | N/A |

(Continued on next page)

Continued

| REAGENT or RESOURCE | SOURCE | IDENTIFIER |
|------------------------------------------------------------|--------------------------|------------|
| HiLoad Superdex 75 10/300 column | Cytiva | 17517401 |
| 3 kDa spin column | Cytiva | 28932218 |
| 4–15% Mini-PROTEAN TGX Gels | BioRad | 4561084 |
| Typhoon 9400 Variable Mode Imager | Molecular Dynamics | N/A |
| Bioruptor Pico | Diagenode | N/A |
| Protein G Dynabeads | Thermo Fisher Scientific | 10004D |
| Flexible orthotopic injection needle (RN NDL 6/PK (33/*)S) | Hamilton | 7803–05 |
| Endoscopic telescope | Wolfe | 8626.431 |
| HD endoscopic camera head | Storz | N/A |

EXPERIMENTAL MODEL AND STUDY PARTICIPANT DETAILS

Cells

To model MSI and CIN CRCs, we previously developed CRISPR mutations in the MC38 mouse CRC cell line.⁹ MSI is modeled by deletion of *Mlh1*, a gene silenced in the majority of sporadic MSI CRCs.⁶ CIN is modeled by an activating Kras mutation (*Kras*^{mut}), as is present in 40% of CRCs² or deletion of *Rad51*, a gene with expression at low or undetectable levels in 88% of CRCs.⁴ Mutated cells were cultured continuously for 6 months before use to allow accumulation of mutations consistent with each CRC subtype. Cells were cultured in DMEM (10% FBS, 1% Penicillin/Streptomycin, 1% HEPES) at 37°C with 5% CO₂.

BMDCs were generated as previously described.⁵⁰ Femur and tibia bones were harvested from C57BL/6 mice and bone marrow was flushed out with PBS. After a PBS wash, cells were plated in non-tissue culture treated plates at 5x10⁶ cells/8mL BMDC growth media (RPMI, 10% supernatant from B16-GMCSF cells, 5% FBS, 10mM HEPES, 1% Penicillin/Streptomycin, 50uM β-Mercaptoethanol). 8mL fresh media was added at days 3 and 5, and non-adherent cells were collected and frozen down for use on day 7. *Sting* knockout BMDCs were generated from *Sting*^{Gt} mice (JAX:017537).

For T cell isolation, the spleen and lymph nodes were collected from OT-1 C57BL/6 (JAX: 003831) mice before negative selection for CD8⁺ T cells using the EasySep Mouse CD8⁺ T cell Isolation Kit (StemCell) as per manufacturer instructions.

Human CRC organoids

Human CRC organoids were generated from resected tumors as described previously.^{9,51} Briefly, tumors were dissociated for 1 h at 37°C in DMEM with 2.5% FBS, 75 U/ml Collagenase XI (SigmaAldrich), 125 µg/mL Dispase II (SigmaAldrich). Following filtration, cells were plated at 500–1000 per well in growth factor reduced Matrigel (Corning) and cultured in basal crypt media (Advanced DMEM/F12 containing 10% FBS, 2 mM Glutamine, 10 mM HEPES, 1 mM N-Acetylcysteine, 1X N2 supplement, 1X B27 supplement, 10 mM Nicotinamide, 500 nM A83-01, 10 µM SB202190, 50 ng/mL EGF) (ThermoFisher) mixed 1:1 with conditioned supernatant from L-cells expressing Wnt3a, R-Spondin and Noggin (ATCC #CRL-3276).⁵² All work with human samples was approved by the Health Research Ethics Board of Alberta Cancer Committee and carried out after obtaining informed patient consent.

Primary MSI variants of the organoids were generated previously using lentiviral transduction with the pLKO.1 system.^{9,53–55} Briefly, organoids were pretreated for 4–5 days with 10 mM Nicotinamide, dislodged from the plate by pipetting, and treated for 5 min at 37°C with TrypLE Express (Life Technologies). Organoids were mixed with concentrated lentivirus along with 8 µg/mL Polybrene and 10 µM Y27632 (SigmaAldrich) and seeded into a 96-well plate. The plate was centrifuged for 60 min at 600 g at 32°C and then incubated at 37°C for 6 h. The organoids were then embedded in Matrigel and cultured in media containing 50–100 µg/mL Hygromycin (Invitrogen) to select for successful transduction. Gene knockdown was verified by western blot.

Mice

C57BL/6 mice originally purchased from Charles River and C57BL/6 OT-1 mice originally purchased from Jackson Laboratory were bred and maintained at the Cross Cancer Institute vivarium. *Sting*^{Gt} mice were purchased from Jackson Laboratory (JAX:017537). Mixed groups of male and female littermates 10–30 weeks old were used for experiments. All animal work was approved by the Cross Cancer Institute's Animal Care Committee.

METHOD DETAILS

CyDNA isolation

CyDNA was isolated as previously described.⁵⁶ Briefly, 5 × 10⁶ MC38 cells were collected by trypsinization before extraction of the cytosolic fraction by incubation in cytosolic extraction buffer (150mM NaCl, 50mM HEPES, 200µg/mL Digitonin, 1M Hexylene Glycol) for 10 min on ice and centrifugation at 2000g for 10 min at 4°C. The supernatant was collected and cytosolic protein and RNA was

then removed by Proteinase K (1 mg/mL at 55°C for 1 h, Fisher) and RNase A (500 µg/mL at 37°C for 1 h, Invitrogen) treatment, each of which were followed by phenol/chloroform/isoamyl alcohol extractions. γ-IR and oxaliplatin concentrations and time points for cy-DNA isolation were confirmed to be non-lethal by crystal violet assays. To isolate cyDNA from patient organoid cultures, 24 confluent wells of organoids were collected using 0.5mL/well Cell Recovery Solution (Corning) on ice. After spinning down at 500g for 5 min at 4°C, cells were resuspended in 3mL TrypLE Express (Life Technologies) and incubated for 5 min at room temperature. Following PBS wash, cells were resuspended in a modified cytosolic extraction buffer (150mM NaCl, 50mM HEPES, 100µg/mL Digitonin, 1M Hexylene Glycol), and the remainder of the cyDNA isolation procedure outlined above was performed. Confirmation of undetectable mitochondrial and nuclear contamination was performed by western blot of the cytosolic and pelleted fractions before protein removal. cyDNA sequences were deposited in the NCBI Sequence Read Archive: PRJNA1152723.

BMDC uptake of endogenous CRC DNA

DNA in the CRC cells was labeled with the Click-iT Edu Cell Proliferation Kit (ThermoFisher). CRC cells were then cocultured at a 1:1 ratio with BMDCs for 4 h and analyzed for uptake of CRC DNA by flow cytometry on the CytoFlex S flow cytometer (Beckman Coulter). Analysis was performed in FlowJo.

BMDC CyDNA stimulations

BMDCs were thawed at 37°C for 3 min and resuspended in RPMI (10% FBS, 1% HEPES, 1% Penicillin/Streptomycin, 50µM β-Mercaptoethanol) before plating 0.5 x 10⁶ cells/2mL in 24 well plates. BMDCs were then stimulated using 1000ng (Figures 5B and 5C) or 500ng (all other stimulation figures) DNA and 0.125µL/mL Lipofectamine 2000 (Invitrogen) as per manufacturer instructions. For pulse stimulations (Figures 1F, 1G, S1E, S1F, and S1H), BMDCs were stimulated in 2mL tubes and stimuli containing media was removed after 15 or 30 min as indicated before PBS wash and plating. DNA oligos were annealed by combining 20µM of each oligo, 10µL NEB Buffer 2, and up to 100µL nuclease free H₂O before incubation at 95°C for 4 min, 70°C for 10 min, and slow cooling to room temperature overnight. PicoGreen staining of cyDNA (Figure S1D) was performed at 37°C for 2 h at 8µL/mL. In stimulations utilizing RU-521, BMDCs were pretreated for 18 h and throughout the stimulation at 3µM. For IN-3, BMDCs were pretreated for 0.5 h and throughout the stimulation at 10µM. For isolation of protein, PBS washed BMDCs were lysed in lysis buffer (50mM Tris-HCl pH 7.5, 150mM NaCl, 50mM Sodium Pyrophosphate, 1mM EDTA, 0.5% NP40, 1% Triton X-100, 2mM Sodium Orthovanadate, 1% Protease Inhibitor (Sigma)) and incubated for 30 min at 4°C on a rotisserie and centrifugation at 18300g for 15 min at 4°C to pellet and remove lipids. Protein concentration was evaluated via the Pierce BCA Protein Assay Kit (Thermo Scientific) and 2-10µg of protein was loaded onto SDS-PAGE gels for western blot analysis.

To assess gene expression, RNA was isolated using TRIzol (Invitrogen) and reverse transcribed with the High-Capacity cDNA Reverse Transcriptase Kit (Applied Biosystems). qPCR reactions were performed using the QuantStudio 6 Real-Time PCR System (Applied Biosystems) with the primers indicated and PowerUp SYBR Green Master Mix (Applied Biosystems). All data shown is normalized to GAPDH unless otherwise stated. All graphs were made in GraphPad Prism 8 and all figures were organized in Inkscape.

BMDC and T cell Co-cultures

5x10⁴ BMDCs were plated in 96 well plates in 50µL RPMI (10% FBS, 1% HEPES, 1% Penicillin/Streptomycin, 50µM β-Mercaptoethanol) and stimulated with 12.5–50ng DNA and 0.125µL/mL Lipofectamine 2000 (Invitrogen) as per manufacturer instructions and 0-5µg/mL OVA protein (Millipore Sigma) for 30 min. BMDCs were then washed 3 times with warm PBS before addition of 1x10⁵ OT1 CD8⁺ T cells (2:1 T cell to BMDC ratio) and incubation at 37°C for 24–48 h. Cells were restimulated for 4 h with 0.5µg/mL PMA, 50µg/mL Ionomycin, and 2 h 2µM Monensin before flow cytometry using the antibodies listed, Zombie Aqua Fixable Viability Kit (BioLegend), and the FOXP3/Transcription Factor Staining Kit (eBioscience) and run on the CytoFlex S flow cytometer (Beckman Coulter). Analysis was performed in FlowJo.

CyDNA Separation by FPLC

CyDNA samples were separated by size exclusion chromatography using a HiLoad Superdex 75 10/300 column (Cytiva) pre-equilibrated with FPLC buffer (20mM HEPES, pH 7.5, 100mM KCl, 1mM EDTA). With each run, 1 mL of sample was loaded onto the column and eluted at 0.65 mL/min with FPLC buffer. Peak fractions were pooled and concentrated using a 3 kDa spin column (Cytiva) and used in BMDC stimulations.

cGAS oligomerization

Following BMDC stimulation as outlined above, protein was instead collected in non-denaturing lysis buffer (50mM HEPES, 150mM NaCl, 10% glycerol, 2mM EDTA, 0.5% Triton X-100) before addition of 5X non-denaturing loading dye (0.25M Tris-HCl pH6.8, 30% glycerol, 0.25% bromophenol blue, 1% deoxycholate). 2-10µg of protein was run on 4–15% BioRad Mini-PROTEAN TGX Gels pre-run at 40 mA for 30 min in non-denaturing running buffer (0.025M Tris-HCl, 0.192M glycine) with 0.2% deoxycholate in the cathode chamber before performing western blot analysis.

Electrophoretic mobility shift assay (EMSA)

EMSA was performed as described in.⁴² 1pmol of DNA oligo was combined with the indicated concentration of recombinant human cGAS protein (Cayman Chemicals) in EMSA buffer (150mM NaCl, 20mM HEPES) for a final volume of 10µL before incubation for 30 min at room temperature. On ice, 1µL of 10X BlueJuice Gel Loading Buffer (Invitrogen) was added before loading onto a 2% agarose gel at 4°C. Gels were then run at 4°C in 0.5X TBE before staining in 1/10000 SYBR Gold (ThermoFisher Scientific) for 1 h at room temperature on a rocker and visualization on the Typhoon 9400 Variable Mode Imager using the A⁴⁸⁸ channel.

MtDNA depletion and isolation

To deplete mtDNA, MSI and CIN cells were treated with 150 ng/mL EtBr for 7 days before cyDNA isolation. mtDNA was isolated using the Mitochondrial DNA Isolation Kit (Abcam) followed by the Qiaprep Spin Miniprep Kit (Qiagen). Genomic DNA was isolated via the GeneJet Genomic DNA Purification Kit (Thermo Scientific). Sonication was performed using the Bioruptor Pico (Diagenode) with 25 cycles of 30 s on, 30 s off. mtDNA was quantified by qPCR using mtDNA-specific primers, converting CTs to expression values, and normalizing to total cyDNA quantity determined by Qubit ssDNA Assay Kit.

Microsatellite CyDNA pulldown

Pulldown protocol was modified from.⁵⁷ 5µg MSI cyDNA was blunted and terminal phosphates confirmed using the NEB Quick Blunting Kit, before ligation to microsatellite expansion adapters containing an EcoRV restriction site using the T4 DNA Ligase Kit (NEB) at a 5:1 ratio overnight at 16°C. Single stranded adapters were previously annealed to double stranded by combination of 20µM of each oligo, 10µL NEB Buffer 2, and nuclease free H₂O to 100µL and incubation at 95°C for 4 min, 70°C for 10 min, and slow cooling to room temperature overnight. After purification of DNA by phenol/chloroform/isoamyl alcohol extraction, microsatellites were pulled down using biotinylated microsatellite probes (containing 5 repeats) as follows. EasySep Streptavidin magnetic beads (StemCell) were washed in 100µL 6X SSC (For 20X SSC: 3M NaCl, 0.3M sodium citrate) 3 times before incubation overnight on a rotisserie at 4°C in blocking buffer (2% BSA, 0.5% SDS, PBS). After another 3 washes in 100µL 6X SSC, beads were resuspended in 100µL 6X SSC. Purified DNA was then hybridized with the biotinylated DNA probes by combining 10µg DNA, 500pmol probe, 60µL 6X SSC, and nuclease free H₂O to 100µL. This mixture was heated to 95°C for 10 min and then incubated at hybridization temperature (approximately 8°C below probe T_m) for the specific probe used (CA, TC, TG: 15°C, TGG: 53°C, GTT: 34°C, GGAA: 55°C). Following this incubation, samples were always kept on ice or at 4°C. The DNA hybridization mixture was then combined with the beads and incubated on the rotisserie for at least 20 min at 4°C. The hybridization mixture was then removed from the beads before bead washing on the rotisserie for 5 min with 200µL 3X SSC twice, 200µL 2X SSC twice, 200µL 1X SSC twice, and resuspended in 30µL nuclease free H₂O. Beads were then incubated at 70°C for 10 min on a shaking heat block and the supernatant containing the pulled down microsatellite cyDNA was collected. As this collected DNA is single stranded, PCR was performed using the Q5 High-Fidelity DNA Polymerase Kit (NEB) and primers specific for the microsatellite expansion adapters (1X Q5 Reaction Buffer, 200µM dNTPs, 0.4µM each primer, 100ng template, 0.02U/µL Q5 High-Fidelity DNA Polymerase) (Cycling conditions: 98°C for 5 min, 35 cycles of: 98°C for 30 s, 69°C for 30 s, and 72°C for 30 s, and final extension at 72°C for 2 min). Adapter sequences were then removed by restriction digest (PCR reaction product, 1X rCutSmart NEB Buffer, 5 U EcoRV-HF (NEB)) at 37°C for 1 h, then 20 min at 65°C. Phenol/chloroform/isoamyl alcohol extraction was performed for final DNA purification. Experimental schematics in Figures 6C, 7A, and S5A were made using BioRender.

cGAS pulldown

For examination of microsatellite binding to cGAS, Protein G Dynabeads (Invitrogen) were washed 3 times in blocking solution (PBS, 0.5% BSA) and incubated with 0.4µg of cGAS or IgG antibodies overnight at 4°C on a rotisserie. Beads were then washed 3 times in blocking solution. 2x10⁷ BMDCs were plated in 6 well plates before stimulation with 2µg DNA and 0.125µL/mL Lipofectamine 2000 (Invitrogen) as described by the manufacturer. Cross links were formed by addition of formaldehyde to the media for a final concentration of 1%, incubated for 10 min, and quenched using glycine at a final concentration of 0.125M. The cytosolic fraction was then isolated by resuspension of cells in cytosolic extraction buffer and incubation on ice for 15 min before centrifugation for 10 min at 2000g at 4°C. The cytosolic fraction in the supernatant was then collected. An aliquot was removed for the whole cytosolic fraction control and the remaining lysate combined with the beads. This mixture was then incubated overnight at 4°C on a rotisserie. Beads were washed 5 times with wash buffer 1 (50mM HEPES, 500mM LiCl, 1mM EDTA, 1% NP40, 0.7% Na-Deoxycholate) and twice with wash buffer 2 (TE, 50mM NaCl). Protein complexes were eluted (50mM Tris-HCl pH 8, 10mM EDTA, 1% SDS) by incubation for 1 h at 65°C on a shaking heat block. Cross links were reversed from pulldown and whole cytosol samples by overnight incubation at 65°C. After addition of TE, samples were incubated with RNase A (Invitrogen) at 0.2 mg/mL for 2 h at 37°C, then Proteinase K (Fisher) at 0.2 mg/mL for 30 min at 55°C before phenol/chloroform/isoamyl alcohol extraction.

Adoptive BMDC transfer

On day 1, 2x10⁵ CIN MC38 cells were injected orthotopically into the descending colon wall, as performed previously, using a flexible needle (Hamilton) inserted through the working channel of a Wolfe endoscope and visualized using the ColoView imaging system.⁵⁵

Fresh BMDCs were prepared as described above. Following collection of non-adherent cells, BMDCs were CFSE stained at a ratio of 1x10⁷ BMDCs/1µM CFDA (Thermo Fisher Scientific) for 10 min at room temperature. BMDCs were then resuspended in RPMI

(10% FBS, 1% Penicillin/Streptomycin, 1% HEPES, 50 μ M β -Mercaptoethanol) and allowed to recover for 30 min at 37°C. Following 2 PBS washes, BMDCs were resuspended in RPMI at 2x10⁶ cells/mL and stimulated using 2 μ g DNA and 0.125 μ L/mL Lipofectamine 2000 (Invitrogen) per 2x10⁶ cells for 30 min at 37°C as per manufacturer instructions. After 2 PBS washes, 2x10⁶ BMDCs were injected intraperitoneally into tumor bearing mice on days 1, 6, and 12.

On day 15, tumors, mesenteric lymph nodes, and spleens were collected, minced, and digested shaking for 30 min at 37°C in enzyme cocktail (RPMI, 10 μ g/mL DNase I (Thermo Scientific), and 1 mg/mL Collagenase IV (Sigma Aldrich)). Tissue was then vigorously pipetted to dissociate and filtered through a 100 μ m (tumor) or 40 μ m (mesenteric lymph node or spleen) strainer before ACK buffer (150mM Ammonium Chloride, 10mM Potassium Bicarbonate, 0.1mM EDTA, pH 7.4) removal of red blood cells (spleen only) and washing. Cells were restimulated for 4 h with 0.5 μ g/mL PMA, 50 μ g/mL Ionomycin, and 2 h with 2 μ M Monensin before flow cytometry staining using the antibodies listed, the Zombie Aqua Fixable Viability Kit (BioLegend), and the FOXP3/Transcription Factor Staining Kit (eBioscience). Stained samples were run on the CytoFlex S flow cytometer (Beckman Coulter). Analysis was performed in FlowJo.

QUANTIFICATION AND STATISTICAL ANALYSIS

All statistical details for experiments can be found in the figure legends. Significance was defined as $p < 0.05$ following paired or unpaired t-tests, or two-way ANOVA as indicated. $n = 3$ refers to experimental replicates, with one representative replicate shown in the figure unless otherwise stated. Each experimental replicate was performed with separate isolations of BMDCs, OT-1 T cells and cyDNA.

scRNASeq

scRNASeq was previously published by us on orthotopically grown MSI and CIN CRCs and deposited as NCBI Gene Expression Omnibus: GSE178706.⁹ Gene signature expression analysis (GSEA) was performed as in the original publication to identify Gene Ontology (GO) signatures associated with each CRC subtype.⁵⁸

Sequencing

CyDNA isolated from MSI and CIN MC38 cells following γ -IR or 5-FU (Sigma-Aldrich) treatment was sequenced by Lucigen using the Mini-Y Adapter Library kit specialized for small DNA strands. Genomic mapping to mouse GRCm38 and RepeatMasker analysis was performed by Lucigen. Read quality was evaluated by Python Bio.SeqIO⁵⁹ and FastQC.⁶⁰ Rsamtools⁶¹ in Bioconductor was used for BAM file analysis of chromosome mapping. NCBI RefSeq gene annotations were downloaded from UCSC and compared to mapping data using rtracklayer⁶² and GenomicRanges⁶³ in Bioconductor. Expected gene, exon, and intron coverage in the genome was taken from Yue et al.⁶⁴ Before analysis of unmapped reads, reads identified as non-mouse with BLASTn (Database: Nucleotide collection (nr/nt), Organism: exclude *Mus musculus*, Expect Threshold: 0.01, Optimize for: Highly similar sequences (megablast), Percent Identity Filter >99%, Query Alignment Start Filter 1–10) were removed to filter out contaminating bacterial and vector reads from the sequencing kit using Python. Filtering by this method removed 96.8% of contaminating reads. Filtered reads were then paired using BBMerge⁶⁵ on default settings. Therefore, unmapped read analysis was performed on all reads that BLAST identified as mouse or failed to align with DNA of other organisms using the high BLASTn thresholds listed above. GC content and local composition complexity was evaluated using Bio.SeqUtils and BioSeqIO in Python.⁵⁹ 2–6 bp microsatellites were identified by MicRoCounter²⁹ and had to repeat a minimum of 5 times to be counted. 1bp microsatellites were identified using Python and Bio.SeqIO by looping through each base in each read and determining if the following base matched. If the following >4 bases were the same as the current base iteration, the sequence was considered a mono-base microsatellite and these bases were skipped before the loop continued. IR and 5-FU graphs with data combined from all subtypes contain 2 clones of MSI cells (Δ MI $h1$), 4 CIN cell types (2 *Kras*^{mut} clones, Δ Rad51, unmutated MC38 CRISPR vehicle control), and *Pole* deficient (Δ Pole).